Iida Sieranen

Fuel-induced corrosion: Analysis of temperature effect on carbon steel immersed in various fuels

School of Technology and Innovations
Master's thesis in Energy Technology
Master's Programme in Smart Energy

Vaasa 2025

Preface

This master's thesis was done in the fuel laboratory of the University of Vaasa.

I thank Neste Oyj for providing Renewable Diesel (RD) and Light Fuel Oil (LFO) for the research.

I acknowledge and thank senior researcher Katriina Sirviö for an interesting master's thesis subject. With this study I have improved my skills significantly with scientific research in fuel-induced corrosion. Thank you for your guidance, help, humor and cheering.

I thank professor Xiaoshu Lü for the review and feedback of my master's thesis.

I commend laboratory engineer Jonna Kaivosoja for assisting with my laboratory work and practical implementations of the immersion tests. Your support, encouragement and presence helped me to complete my master's thesis.

I thank senior researcher Carolin Nuortila for her help with scanning electron microscope (SEM) images. Your assistance and expertise eased the implementation of the master's thesis. Project researcher Huaying Wang-Alho thank you for helping with the practical implementation. Your calculations and skills were an important part for this study to succeed.

Finally, I would like to thank my family for their solid support during my studies. I thank my sister Sofia and my father Kalervo for critical feedback for my master's thesis. I thank Manta for the long walks, which became necessary in many challenging situations. My last thanks go to my husband Emppu for everything.

Espoo 01.02.2025

Iida Sieranen

UNIVERSITY OF VAASA
School of technology and innovations
Author: Iida Sieranen
Title of the Thesis: Fuel-induced corrosion: Analysis of temperature effect on carbon steel immersed in various fuels
Degree: Master of Science
Programme: Master's Programme in Smart Energy
Supervisor: Xiaoshu Lü
Instructor: Katriina Sirviö
Year: 2025 **Number of pages:** 86

ABSTRACT:
The European Union (EU) aims to phase out fossil fuels by 2050. Shipping involves transportation of passengers or merchandise. Shipping, one of the largest sources of greenhouse gas emissions, must transition to alternative fuels. Alternative fuels such as hydrogen, ammonia, methanol (MeOH), hydrotreated vegetable oil (HVO) and their blends are possible fuels for future maritime applications to replace fossil fuels.

The compatibility of alternative fuels and engine materials creates a challenge for maritime applications. Internal combustion engine (ICE) materials, like various metals, have different corrosion resistances. Corrosion resistance and the compatibility of materials can be studied using several methods. The fuel passes through the ICE from the tank through the entire fuel system. Anywhere fuel flows the material compatibility of alternative fuels must be ensured.

The first objective of this study was to improve the University of Vaasa's Fuel laboratory's immersion test initial setting. The improvement of the immersion test was developed in sectors: the metal sample size, the method of attaching the metal sample to the sample container, the preparation of the fuel blend, the effect of temperature and scanning electron microscope (SEM) images. The second objective of this thesis was to implement the improved immersion test and examine the compatibility of various fuels with carbon steel (CS). The test was performed at two different temperatures of 23 °C and 40 °C, for over 300 hours, to examine the effect of temperature on the formation of corrosion. The studied fuels were Renewable Diesel (RD) and light fuel oil (LFO), both without additives, MeOH, and the blend of RD, and MeOH, stabilized with 1-octanol (later blend), containing 8 % of MeOH based on the energy ratio. The possible corrosion was studied by analyzing the fuels' trace metals concentrations before and after the test and analyzing the CS samples visually and by SEM. In addition, the properties of the studied fuels were analyzed before and after the immersion test.

As a result of this thesis the improvement of the immersion test enables more detailed research results. According to the trace metal concentration analyses results, no contamination caused by the CS plates was found in any of the studied fuels. SEM images and visual observation of the samples support this result as no signs of corrosion were detected on the CS samples. The temperature did not affect fuel contamination and corrosion. The measured results of kinematic viscosity and density for RD, blend and LFO met the requirements of the standards. According to the distillation results, RD and LFO met the requirements of the standards. Neither the temperature change nor the immersion of the CS samples on the fuels changed the fuel properties.

KEYWORDS: Corrosion, analysis methods, carbon steel, immersion test, fuel

VAASAN YLIOPISTO
Tekniikan ja innovaatiojohtamisen yksikkö
Tekijä: Iida Sieranen
Tutkielman nimi: Polttoaineen aiheuttama korroosio: Tutkimus lämpötilan vaikutuksesta eri polttoainelaatuihin upotettuun hiiliteräkseen
Tutkinto: Diplomi-insinööri
Oppiaine: Sähkö- ja energiatekniikka
Valvoja: Xiaoshu Lü
Ohjaaja: Katriina Sirviö
Valmistumisvuosi: 2025 **Sivumäärä:** 86

TIIVISTELMÄ:
Euroopan Unioni (EU) pyrkii luopumaan asteittain fossiilisten polttoaineiden käytöstä vuoteen 2050 mennessä. Laivaliikenne on yksi suurimmista kasvihuonepäästöjen aiheuttajista. Laivaliikenteen on siirryttävä käyttämään vaihtoehtoisia polttoaineita. Vaihtoehtoiset polttoaineet kuten vety, ammoniakki, metanoli (MeOH), vetykäsitelty kasviöljy (HVO) ja niiden seokset ovat mahdollisia korvaajia tulevaisuuden laivaliikenteen polttoaineina fossiilisten polttoaineiden sijaan.

Vaihtoehtoisten polttoaineiden ja moottoreiden materiaalien yhteensopivuus luo haasteen laivateollisuudelle. Polttomoottorin materiaalit kuten erilaiset metallit omaavat erilaiset korroosion kestävyydet. Korroosion kestävyyttä ja materiaalien yhteensopivuutta voidaan tutkia monella menetelmällä. Polttoaine kulkee läpi polttomoottorin, alkaen tankista koko polttoainejärjestelmän läpi. Vaihtoehtoisten polttoaineiden ja järjestelmän materiaalien yhteensopivuus tulee varmistaa kaikkialla, missä polttoaine virtaa.

Tämän tutkimuksen tavoitteena oli kehittää Vaasan yliopiston polttoainelaboratorion upotuskoemenetelmää. Upotuskoemenetelmää kehitettiin seuraavilla osa-alueilla: metallinäytteen koko, metallinäytteen kiinnitysmenetelmä näyteastiaan, polttoaineseoksen valmistus, lämpötilan ja pyyhkäisyelektronimikroskooppi- eli SEM-kuvien vaikutus. Työn toisena tarkoituksena oli tutkia eri polttoaineiden yhteensopivuutta hiiliteräksen kanssa parannettua upotuskoemenetelmää käyttäen. Testi suoritettiin kahdessa eri lämpötilassa, 23 ja 40 °C:ssa. Molempien kokeiden kesto oli yli 300 tuntia. Tutkimuksen tavoitteena oli selvittää, vaikuttaako lämpötilan muutos korroosion ilmenemiseen. Tutkitut polttoaineet olivat uusiutuva diesel (RD) ja kevyt polttoöljy (LFO), molemmat ilman lisäaineita, MeOH:n ja RD:n seos, joka oli lisäaineistettu 1-oktanolilla seoksen vakauttamiseksi (myöhemmin seos). MeOH:n ja RD:n seos sisälsi energiasisällön perusteella 8 % MeOH:a. Mahdollista korroosiota tutkittiin analysoimalla polttoaineiden alkuainepitoisuudet ennen upotuskoetta ja sen jälkeen sekä arvioimalla hiiliteräslevyt visuaalisesti sekä SEM-kuvilla. Lisäksi tutkittujen polttoaineiden ominaisuudet analysoitiin ennen upotuskoetta ja sen jälkeen.

Upotuskoemenetelmän kehittäminen mahdollistaa tarkemmat tutkimustulokset. Alkuaineanalyysien tulosten perusteella tutkituista polttoaineista ei löytynyt hiiliteräslevyjen aiheuttamaa kontaminaatiota. SEM-kuvat ja näytteiden visuaalinen havainnointi tukevat tätä tulosta, koska hiiliteräslevyissä ei havaittu merkkejä korroosiosta. Lämpötilan muutos ei vaikuttanut polttoaineen kontaminaatioon ja korroosioon. RD, seos ja LFO täyttivät standardien vaatimukset tiheyden ja kinemaattisen viskositeetin mittaustulosten osalta. Tislaustulosten mukaan RD ja LFO täyttivät standardien vaatimukset. Lämpötilan muutos tai hiiliteräslevyn upottaminen polttoaineisiin eivät muuttaneet polttoaineiden ominaisuuksia.

AVAINSANAT: Korroosio, analyysimenetelmät, hiiliteräs, upotuskoe, polttoaine

Table of contents

Figures

Tables

Symbols and Abbreviations

Symbols

A	Surface Area
CR	Corrosion Rate
n	Number of the Observation
RSD	Relative Standard Deviation
s	Sample Standard Deviation
t	Time
V	Volume
X	Corrosion Rate in mpy unit
$\overline{x}$	Arithmetic Mean
x_i	Individual Observation Value
Δm	Mass loss
ρ	Density

Abbreviations

AAS	Atomic Absorption Spectrometry
Ag	Silver
Al	Aluminum
ASTM	American Society for Testing Materials
Au	Gold
bar	Unit for pressure (1 bar = 100 kPa)
Blend	Methanol and renewable diesel fuel blend with 1-octanol as additive
C	Carbon

Ca	Calcium
Cd	Cadmium
CH_3OH	Methanol
CI	Compression Ignition
Cl	Chlorine
cm^2	Squire centimeter
cm^3	Cubic centimeter
CO	Carbon Oxide
Co	Cobalt
CO_2	Carbon dioxide
Cr	Chrome
CTOD	Crack Tip Opening Displacement
Cu	Copper
e-	Negatively charged electron
EDS	Energy Dispersive Spectroscope
ETIP	European Technology and Innovation Platform
EU	European Union
FBP	Finale Boiling Point
Fe	Iron
g	Gram
GAF	Gaseous Alternative Fuels
g/cm^3	Gram per cubic centimeter
h	Hour
Hg	Mercury
HVO	Hydrotreated Vegetable Oil
H_2	Hydrogen
H_2O	Water
H^+	Positive hydrogen ion
IBP	Initial Boiling Point
ICE	Internal Combustion Engine

ICP-OES	Inductively Coupled Plasma Optical Emission Spectroscopy
ISO	International Organization for Standardization
K	Potassium
kg/m^3	Kilogram per cubic meter
LFO	Light Fuel Oil
LHV	Lower Heating Value
Li	Lithium
MeOH	Methanol
Mg	Magnesium
mg/kg	Milligram per kilogram
MJ/kg	Megajoules per kilogram
ml	Milliliter
mm	Millimeter
mm^2/s	Squire millimeter per second
Mn	Manganese
Mo	Molybdenum
mpy	Mils per year
Na	Sodium
NaCl	Sodium Chloride
NEXBTL	Next Generation Biomass to Liquid
NH_3	Ammonia
Ni	Nickel
NO_x	Nitrogen Oxide
N_2	Nitrogen
N_2O	Nitrous Oxide
n/a	Not analyzed
OM	Optical Microscope
O_2	Oxygen
OH^-	Hydroxide
P	Phosphor

Pb	Lead
Pd	Palladium
PEM	Poly Electrolyte Membrane
PM	Particulate Matter
ppm	Part per million
Pt	Platinum
RD	Renewable Diesel
S	Sulphur
SEM	Scanning Electron Microscope
SI	Spark-ignition
Si	Silicon
Sn	Tin
V	Vanadium
WWFC	The Worldwide Fuel Charter
XPS	X-ray Photoelectron Spectroscope
XRD	X-ray diffraction
Zn	Zinc
µm/year	Micrometer per year
ºC	Celsius
%	Percent

1 Introduction

According to the European parliament (2022) shipping means transportation of passengers or merchandise. Shipping is one of the fastest growing sources of greenhouse gas emissions. Shipping uses a considerable quantity of fossil fuels. There is a need to replace fossil fuels, and the solution could be found in alternative fuels. The European Union (EU) has set the target by the year 2030 to reduce greenhouse gas emissions by 55 % in EU region. By 2050 the target is to reach net zero in terms of shipping greenhouse gas emissions. The EU target is to increase the count of environmentally sustainable fuels and their initialization on maritime applications.

Among the possible alternative fuels that will be used in maritime applications in the future are hydrogen (H_2), ammonia (NH_3), methanol (MeOH) and hydrotreated vegetable oils (HVO) and their blends (Det Norske Veritas, 2024). The adoption of alternative fuels requires careful consideration of factors affecting corrosion, as these can significantly impact engine components (Foretich et al., 2021, pp. 2, 7, 9). Corrosion causes challenges for the normal function of internal combustion engine's (ICE) (Hänninen et al., 2022, p. 172).

Alternative fuel production methods, use and corrosion as a phenomenon are presented in the literature review of this study. In the literature review, alternative fuels are reviewed more comprehensively. The experimental part of this study has been executed for conventional reasons on selected liquid fuels. The University of Vaasa's Fuel laboratory enables the research of liquid fuels.

The formation of corrosion can be examined using multiple different methods. In the literature part of this study, two methods are reviewed: the immersion test and the electrochemical method. Shehzad et al. (2021, pp. 2–3) viewed the current trends to execute the immersion test. In the immersion test the metal sample is immersed in the fuel being studied for a certain period and thus causes corrosion. In the electrochemical method corrosion is induced in the examined metal with the help of an electric current.

The immersion test is more popular way to study corrosion in scientific research, because it can be used to consider the effect of the fuel on the metal being studied.

The first objective of this study was to improve the University of Vaasa's Fuel laboratory's immersion test initial setting. The second objective was to implement the improved method by studying the compatibility of various fuels with carbon steel (CS) and to examine the effect of temperature on the formation of corrosion. The studied fuels were renewable diesel (RD), light fuel oil (LFO), MeOH and fuel blend of RD and MeOH with a MeOH content of 8 % based on the energy ratio (later blend). The blend was stabilized by using 1-octanol as an additive. The fuel blend ratio was chosen with the intention to investigate fuel blend that could be useful in certain combustion concepts, and no material compatibility studies have yet been conducted for this blend ratio.

The improvement of the immersion tests was developed in several sectors. The improvement of the immersion test method enables a more detailed examination of the results of corrosion research.

The practical part of this study was to implement an improved method of the immersion tests to practice. The immersion test was conducted at two different temperatures of 23 °C and 40 °C. The CS samples were cleaned and weighed before the immersion tests. Four fuels were involved in the study: RD, MeOH, blend and LFO, or normal fossil diesel which was served as a reference fuel in the study.

After the immersion tests visual observations of the corrosion were made. The CS samples were cleaned and weighed again. The mass loss of the CS samples was calculated based on the weighing results. With mass loss of the samples corrosion rate (*CR*) was calculated. Laboratory analysis methods of the fuels were kinematic viscosity, density, distillation and measurements of the trace metal concentration. Scanning electron microscope (SEM) images were taken from the CS samples to see the surface of the samples in more detail.

2 Overview of maritime fuels

European parliament (2022) professes that shipping is one of the fastest growing sources of greenhouse gas emissions that have a negative impact on climate change. The increase in shipping traffic is due to the increase in passenger traffic and trade. The corona pandemia period temporarily reduced the greenhouse gas emissions from shipping, but according to forecasts, the greenhouse gas emissions will increase in the future. For this reason, the EU has set a goal by 2030 to reduce greenhouse gas emissions by 55 %. In 2050, the goal is to reach net zero in terms of shipping greenhouse gas emissions. The EU aims to regulate shipping emissions by adding maritime transport to the emissions trading system in EU's region. In addition, the EU's goal is to increase the number and initialization of environmentally sustainable fuels.

2.1 Alternative maritime fuels

Det Norske Veritas (2024) attests that the research and introduction of alternative fuels has been accelerated by the tightening of emission restrictions and the rising price of fossil fuels. In the future hydrogen, ammonia, MeOH and HVO will probably replace the fossil fuels currently used as shipping fuel. However, when pondering the usage of alternative fuels for maritime applications operational safety, fuel impact on the design of ICE and possible problems caused by its use, such as corrosion should be considered. Alternative fuel production methods, their impact on the environment and the amount of greenhouse emissions should be examined.

2.1.1 Hydrogen

Zemite et al. (2023, p. 44) state that the most universal chemical element is hydrogen. In nature, hydrogen mostly occurs as compounds with other chemical elements, and therefore hydrogen must be produced. Oy Linde Gas Ab (2024, pp. 2–3, 8) professes that under normal conditions, hydrogen is a colorless, odorless, tasteless and easily explosive gas. The burning flame of hydrogen is hot and almost colorless. Hydrogen is not a

poisonous gas, but it becomes suffocating when its concentration increases. Hydrogen is a very light gas, and its density is 0.089 kg/m^3 (Zemite et al., 2023, p. 44).

Shiva Kumar and Himabindu (2019, pp. 442–443) review state that hydrogen production requires more energy input than it provides. Hydrogen production methods can be divided into two categories based on used energy sources. It can be produced using either fossil or renewable energy and it can be developed by several different methods. The most common way to produce hydrogen is by reforming methane and it creates carbon dioxide (CO_2).

According to the Shiva Kumar and Himabindu (2019, pp. 444–446) review electrolysis of water is the way to produce green hydrogen. The electricity used for electrolysis must be manufactured using renewable energy sources to produce green hydrogen. Oxygen (O_2) and hydrogen are separated from water (H_2O) with the help of electricity (Formula 3). PEM electrolyzer (Poly Electrolyte Membrane) uses polymer membrane technology. At the anode, the PEM electrolyzer separates oxygen and hydrogen from water (Formula 1). The positive hydrogen ion (H^+) moves through the polymer membrane to the cathode side. The disconnected negatively charged electron (e^-) transfers to the cathode side along its own channel. On the cathode side, the positive hydrogen ion and the negatively charged electron meets and combines with each other and forms hydrogen (Formula 2).

$$H_2O \rightarrow 2H^+ + \frac{1}{2}O_2 + 2e^- \quad (1)$$

$$2H^+ + 2e^- \rightarrow H_2 \quad (2)$$

$$2H_2O \rightarrow H_2 + \frac{1}{2}O_2 \quad (3)$$

Durbin and Malardier-Jugroot (2013, pp. 14596–14599, 14601) describe hydrogen as a small molecular gas that easily escapes from storage. There are three methods available to hydrogen storage: high pressure, liquid form and combined with metal hybrids. High pressure special tanks are required when storing hydrogen with high pressure. Pressure reduces the volume of hydrogen as a gas. Hydrogen in liquid form requires a low -253 °C

temperature. Storing hydrogen in liquid form requires a tank with thermal insulation and continuous cooling. The third practice to store hydrogen is to combine it with metal hybrids. There is no commercial application of this storage method. Metal hybrids can bind less than 10 % of their own weight and storage method requires heavy tanks. On the other hand, this storage method is safe, and hydrogen can be released by heating metal hybrids.

Helander (2021) reported hydrogen powered maritime engines development project with the cooperation of several parties. Development of hydrogen-powered passenger ferry and its initialization in the year 2027 is in progress. The challenges of hydrogen in shipping culminate in hydrogen's low energy density. The use of hydrogen as fuel requires large storage tanks on board, which occupy considerably space and weight. This decreases shipping efficiency and creates a challenge for the hydrogen-powered ships design. A considerable amount of energy is lost before hydrogen can be used as a fuel. Hydrogen does not produce greenhouse gas emissions, and the final product is water. Hydrogen also has high efficiency per mass. Hydrogen in liquid form does not cause corrosion, but various compounds of hydrogen, for example, hydrogen sulfide causes corrosion in CS (Tukes, 2024).

Acar and Dincer (2020, pp. 3397–3398, 3404–3405) state that the introduction of hydrogen in shipping requires certain issues to be considered. The problem of hydrogen sustainability for maritime applications is the non-existing infrastructure of gas stations and distribution networks. The safety issues of hydrogen must be solved. Hydrogen can diffuse through many different materials. The blend of hydrogen and oxygen ignites or explodes very easily. Maritime applications would profit coastline location of hydrogen gas pipes. Usage of green hydrogen would be optimal for the environment. It is optimal to use hydrogen from industrial side streams, although it is produced with fossil fuels. Hydrogen needs transportation routes and trade from abroad. Maritime applications need redesign of ICE. Hydrogen usage for maritime applications in the future requires major financial investment.

2.1.2 Ammonia

Cames et al. (2021, pp. 9–10, 40) state that ammonia is one of the potential future alternative fuels in shipping, due to its carbon neutrality. Ammonia is used as a raw material in the fertilizer industry. Ammonia serves as a hydrogen carrier and can be converted into hydrogen-based fuels. Hydrogen has lower energy density than ammonia. Considering ammonia as fuel for shipping, it should not create a competitive situation with food production.

Safety procedures must be considered using ammonia as fuel. VWR BDH Chemicals (n.d.-b, p. 2) professes that ammonia is extremely caustic to the skin and damaging to the eyes. In addition, ammonia can cause irritation in the respiratory system. Ammonia is toxic for aquatic organisms. According to Cames et al. (2021, pp. 9–10, 24) ammonia is a challenging fuel in maritime traffic precisely because of its toxic nature. At normal atmospheric pressure, ammonia gas is a colorless, poisonous and stingy characteristic odor. Ammonia is a moderately safe fuel to use, because it has high octane rate and narrow ignition range (Herbinet et al., 2022, p. 1).

Kyriakou et al. (2017, pp. 2–3) studied the advancements in the field of electrochemical synthesis of ammonia. Ammonia can be produced using the Haber-Bosch method or electrochemical synthesis. Ammonia production with the Harber-Bosch method uses natural gas as raw materials. In practice, when ammonia is produced, nitrogen (N) and hydrogen are combined together, and the final product is ammonia (Formula 4). The Haber-Bosch method is based on steam reforming, which produces a hydrogen-rich gas mixture from natural gas. The hydrogen-containing gas mixture is reformed at high temperature into clean hydrogen. In an ammonia reactor under high pressure, nitrogen and hydrogen are compressed together. The catalyst of the chemical reaction can be iron oxide or metal carbide powder. In the Haber-Bosch method, the raw materials contain carbon (C) compounds.

$$N_2 + 3H_2 \leftrightarrow 2NH_3 \qquad (4)$$

Kyriakou et al. (2017, pp. 2–3, 5) state that electrochemical synthesis is the practice to produce ammonia with renewable energy sources. Electrochemical synthesis requires hydrogen. If hydrogen is produced using renewable energy sources, the production of ammonia is almost emission-free. The electrolyte process requires a temperature of 100-500 °C. A two-chamber reactor has a semiconducting membrane in between. A voltage passes across the membrane. On the side of the hydrogen chamber, the hydrogen is broken down into positive hydrogen ions and negatively changed electrons (Formula 5). Through the membrane, the hydrogen ions move to the side of the nitrogen chamber, which acts as a cathode. In the nitrogen chamber, nitrogen and hydrogen proton combine to form ammonia (Formula 6).

$$3H_2 \rightarrow 6H^+ + 6e^- \quad (5)$$

$$N_2 + 6H^+ + 6e^- \rightarrow 2NH_3 \quad (6)$$

Cames et al. (2021, p. 29) indicate that the ammonia usage in shipping is a promising carbon-neutral fuel. The use of ammonia as a fuel causes other greenhouse emissions such as nitrogen oxide (NO_x), nitrous oxide (N_2O) and ammonia slip, which means unburned ammonia. There are no maritime applications using ammonia as fuel, but several operators are developing an ammonia-powered engine for shipping (Marine & Offshore, 2024).

Cames et al. (2021, pp. 31–32) state that ammonia is mostly stored in liquid form for practical reasons, such as volume reduction and detecting possible leaks. Storage of ammonia in liquid form requires cooling temperature of -33 °C and 1 bar pressure. Alternative solution for ammonia storage is liquid form, which needs pressure tank at temperature of 25 °C and the pressure of 10 bars. Ammonia storage tanks require energy efficiency from the propulsion system. Ammonia is easier to store hydrogen, but there are still major challenges in storage and transportation. Ammonia's lower heating value (LHV) is 19 MJ/kg. Ammonia as fuel for shipping requires quantitatively significantly more fuel than fossil fuel.

Herbinet et al. (2022, pp. 1, 10) confirm that ammonia as fuel can cause corrosion in various metal alloys. The corrosion risk must be considered in the selection and design of engine materials. The use of ammonia creates many technical, environmental and economic challenges. On the other hand, a worldwide distribution infrastructure has already been created for ammonia, although not for maritime applications.

2.1.3 Methanol

MeOH (CH_3OH) is defined as a toxic chemical and it is a colorless and easily flammable fuel with a low flash point (Ellis & Tannberger 2015, p. 2). VWR BDH Chemicals (n.d.-a, p. 1) professes that safety issues from using MeOH must be considered. The safety aspects of MeOH are connected to operational safety to avoid inhalation, ingestion and skin contact. MeOH is easily flammable in liquid and gas forms. MeOH harms several organs.

Ellis and Tannberger (2015, pp. 2, 24) state that MeOH is extensively used in the chemical industry. Several fossils and renewable raw materials can be used in the manufacture of MeOH. Production of MeOH is mostly from natural gas and coal. Production of renewable MeOH can be from pulp mill residue, waste and carbon dioxide.

The method of producing MeOH is called methanol synthesis or hydrogenation reaction (Rufer, 2022, pp. 1). IRENA and Methanol Institute (2021, pp. 42–47) profess that carbon monoxide (CO) or carbon dioxide and hydrogen are needed to create MeOH. Production of renewable MeOH, or e-methanol used hydrogen must be green hydrogen. Green hydrogen is produced by electrolysis from water. The electricity used in electrolysis must be produced using renewable energy sources. The carbon monoxide or carbon dioxide used to generate MeOH can be recovered from industry or directly from the atmosphere. According to Rufer (2022, pp. 1–3, 5) the production of MeOH takes place through three chemical reactions. The chemical reaction requires a catalyst, for example, copper (Cu) or zinc (Zn), a temperature of 200-300 °C and a pressure of 50-100 bar. Chemical reactions can happen in both directions. In direct methanol synthesis, carbon dioxide and hydrogen are directed to a reactor where three chemical reactions take place.

Catalytic hydrogenation of carbon dioxide (Formula 7) is an exothermal chemical reaction in which MeOH and water are formed from carbon dioxide and hydrogen. The water gas shift reaction (Formula 8) is an undesirable reverse reaction. The water gas shift reaction is an endothermal chemical reaction in which carbon dioxide and hydrogen form carbon monoxide and water. The catalytic hydrogenation of carbon monoxide (Formula 9) is an exothermic reaction in which carbon monoxide and hydrogen form MeOH.

$$CO_2 + 3H_2 \leftrightarrow CH_3OH + H_2O \quad (7)$$

$$CO_2 + H_2 \leftrightarrow CO + H_2O \quad (8)$$

$$CO + 2H_2 \leftrightarrow CH_3OH \quad (9)$$

Rufer (2022, p. 7) describes that after the reactor the final products carbon dioxide, carbon monoxide, hydrogen, water and MeOH produced in methanol synthesis go to the condenser from where carbon dioxide, carbon monoxide and hydrogen are recycled back to the reactor. Water and MeOH continue their way to separation, where MeOH is separated from water by distillation.

Ellis and Tannberger (2015, p. 2) state that MeOH as marine fuel enables the reduction of greenhouse gas and carbon dioxide emissions in shipping. MeOH as fuel does not contain sulphur (S) and that's the reason why it is compatible with the European Commission Sulphur Directive. Several ships using MeOH as fuel have already cleared their way to shipping.

Ellis and Tannberger (2015, p. 2) confirm that MeOH has an energy density about half as low as that of ordinary fossil fuel. A lower energy density results in a higher demand for fuel, which is evident in the increased requirement for fuel storage on board ships. MeOH can cause corrosion to different materials, necessitating that the design of tank coatings, pipes, seals, and other components be appropriate for MeOH use.

2.1.4 Hydrotreated Vegetable Oils

HVO is hydrogenated vegetable oils, and it is called renewable diesel (Mussa et al., 2024, p. 1). Neste (2023, p. 2) defines hydrotreated vegetable oils as renewable hydrocarbon, and it is suitable fuel for diesel engines as such or as a blend with fossil diesel. Operation safety must be considered when using HVO, as it can potentially cause death if swallowed or inhaled. Continuous exposure of HVO might cause skin dryness and cracking. HVO is a highly flammable liquid. HVO has the risk of contaminating the environment by pollution of the soil and groundwaters.

Mussa et al. (2024, pp. 1–2) suggest that HVO as a fuel is superior compared to biodiesel and other biofuels, due to its better combustion efficiency, less emissions, better cold and storage properties. HVO absorbs less moisture and lubricates the ICE better compared to other biofuels. The use of HVO as a fuel reduces emissions from exhaust gases, such as carbon dioxide, nitrogen oxides and particulate matter (PM) emissions compared to fossil fuel. The low density and high cetane number are considered the challenges of HVO, for which the ICE should be tuned for blends with a high concentration. When producing HVO, it should not compete with food production.

European Technology and Innovation Platform ETIP Bioenergy (2020, pp. 1–2) profess that feedstock used in HVO production are from biomass-based vegetable oil triglycerides or fatty acids. HVO is produced by hydrogenation and hydrocracking triglycerides with catalysts (Formula 10 and 11). Hydrogen treatment process requires a temperature of 300-390 °C and high pressure. In hydrogen treatment process HVO and propane are produced. Propane can be salvaged and used, for example, as fuel for heating. Hilbers et al., (2015, pp. 652–654) describe that the production of HVO can be divided into different processes: raw material pre-treatment, hydrogen treatment and isomerization. In the pre-treatment impurities are removed from feedstock. In hydrogen treatment oxygen is removed from biological triglycerides, generating paraffins, or straight-chain hydrocarbons. Used feedstock and production conditions affect the properties of the obtained fuel and its molecular structure. In hydrogen treatment,

hydrogen is added to the double bonds of the triglyceride, so that the triglyceride is broken into fatty acids. Fatty acids are transformed into hydrocarbons with hydrodeoxygenation or decarboxylation. In hydrodeoxygenation oxygen and water are removed from fatty acids. In decarboxylation oxygen and carbon dioxide are removed from fatty acids. At the end of the hydrogen treatment, the final product undergoes isomerization, where redundant carbon dioxide and water are removed.

$$RCOOH + 2H_2 \rightarrow R - H + 2H_2O \quad (10)$$

$$C_3H_5(RCOO)_3 + 12H_2 \rightarrow C_3H_8 + 3RCH_3 + 6H_2O \quad (11)$$

Neste (n.d.) defines HVO as a subgroup of RD. Main difference is about raw materials. The raw materials used in the production of RD are not necessarily all plant-based. RD is available as Neste MY renewable diesel fuel for automotive use, which is produced using NEXBTL technology (Next Generation Biomass to Liquid). According to the study of Wang-Alho et al. (2024, pp. 3, 14) the use of HVO in shipping is a promising substitute for fossil fuel because it can be used in the ICE as such. HVO is suitable as a fuel with various metals without causing corrosion. The expensive price of HVO creates a challenge for the initialization of the fuel (Mussa et al., 2024, p. 1).

2.2 Alternative fuels and materials compatibility

The usage of alternative fuels has increased in maritime applications (Det Norske Veritas, 2024). Simultaneously looking for means to moderate the amount of greenhouse gas emissions, also the challenges of material compatibility created by alternative fuels should be considered. Oni et al. (2022, pp. 7509, 7525) verify that metals such as aluminum (Al), copper and mild steel are used in ICE and their corrosion tolerance are different. According to study of the metals mentioned above, copper has the worst corrosion resistance.

Kim and Chun (2023, pp. 1–2, 7, 28–29) studied material compatibility in maritime applications when hydrogen is used as a fuel. According to the study, choosing metal

materials should be regarded on shipboard storage and piping systems. The phase of hydrogen, gas or liquid creates its own challenges for the durability of materials. Material compatibility can be studied with tensile test, charpy impact test, fatigue test, CTOD test (Crack Tip Opening Displacement test) and ductile fracture toughness test. According to the study non-corrosive and low flash point fuels do not require corrosion testing. For example, aluminum as a metal requires corrosion testing. For cryogenic and hydrogen environment stainless steel is compatible material. The concentration rate of nickel increases in austenitic stainless steel, and it raises the mechanical tolerance of the metal. Nickel-rich austenitic stainless steel is the most suitable metal for the demands of the maritime industry, considering the operational requirements, but it might lead to an expensive design. High temperature indicates hydrogen has a more harmful effect on metals than cryogenics conditions have. Recommendation is to perform evaluation of the mechanical performance.

Liu et al. (2022, pp. 1, 4–6, 8, 14–15) studied Gaseous Alternative Fuels (GAF) compatibility with ICE materials performance. In this study GAF includes hydrogen, ammonia and natural gas. ICE materials' performance can be divided into critical engine parts and their malfunctions account of corrosion, thermal damage and detrition. Safety and reliability are considered in ICE material recommendation. Hydrogen seems promising fuel for maritime applications. The challenges caused by hydrogen in the durability of materials can be answered with advanced material choices, manufacturing processes and advanced lubrication, which has a favorable effect on the thermal efficiency and output of the ICE. Hydrogen causes challenges for the combustion chamber, fuel system and lubricating oil. Hydrogen causes corrosion in ICE metals, polymers and lubricant oils. The moving parts of the ICE such as valve-vale seat tribo-system and cylinder liner-piston ring tribo-system are prone to corrosion due to hydrogen.

Hydrogen might cause the ICE thermal load, which may cause thermal damage to the ICE. Melting the upper parts of the piston and deformation of the exhaust valves are

results of engine thermal damage. Hydrogen can weaken the properties of lubricant oils and thus cause detrition in the ICE.

According to the study of Liu et al. (2022, pp. 5, 15) ammonia as a fuel cause challenges to safety storage and reliability. Ammonia weakens the properties of lubricant oils, which are nevertheless within reasonable limits. Engine parts made from copper alloys are at risk of corrosion caused by ammonia. The study proposes several practices to prevent corrosion in ICE. Different fuel blends such as hydrogen and ammonia fuel blend or hydrogen and natural gas fuel blend could be an answer to the corrosion challenge. The development of lubricant oils could help prevent the detrition of materials. For thermal damage, controlling the engine's combustion process is the response to the problem. Engine design, including injection timing and fuel and air ratio assists the combustion process in ICE.

Wang-Alho et al. (2024, pp. 1, 14) studied aluminum, CS, stainless steel and MoC210M/25CrMo4+SH alloys corrosion behavior in HVO with and without additives, MeOH and fuel blends with HVO, MeOH and 1-octanol or 1-dodecanol as adhesive of the fuels. The initial setting of the study was an immersion test duration of 60 days at room temperature. The study results show that slightly increased risk of corrosion is caused by MeOH or its blends. The metals aluminum and CS were slightly soluble in MeOH. The study shows that HVO without or with additives was compatible with the metals under investigation. The visual observation of a corrosion was not detected on the surface of the metals. The fuel properties were not affected by the corrosion that may have formed. HVO as a fuel is suitable for ICE use. Few research has been made of HVO-MeOH blends and the adhesive as fuel and the compatibility of the blend with the metal materials of the ICE. The compatibility of MeOH, its blends and ICE materials should be investigated further.

Shehzad et al. (2021, pp. 1–2, 32) verify that biodiesel causes more corrosion in ICE than fossil fuels. Not all properties that afflict and decelerate corrosion caused by biodiesel

are known. Kuittinen (2012, pp. 16–18, 44–45) states that chlorine and alkali metals contained in biodiesel react in ICE during the combustion process, causing compounds that contribute corrosion. Biodiesel contains more water compared to fossil fuel. This is due to the hydroscopic nature of biodiesel. The water contained in biodiesel is one of the causes of corrosion.

Okokpujie et al. (2023, pp. 1–2, 13–15) study of corrosion and thermal analysis of material and their compatibility for ICE. Review shows that biodiesel and biofuels are compatible with ICE components. According to the study, the current ICE spark ignition (SI) and compression ignition (CI) engines that use fossil fuel require modifications on their design to replace fuel with biodiesel or biofuels. ICE needs modification on its design to elevate effective combustion reactions to decrease carbon monoxide, carbon dioxide and nitrogen oxides emissions. In the ICE design should consider the compatibility of different parts and components design should be compatibility with materials. This would prevent both detrition and corrosion. Alcohols such as ethanol and n-butanol have low cetane number, which causes challenges due to the longer ignition delay of the fuel blends. This leads to noise in the ICE during the combustion process, compared to using diesel. To increase the use of higher blending ratios of biofuels and alcohols in ICE, more research must be done. Ethanol storage and stability challenges must be solved. The production speed and expenses of n-butanol create challenges. The ICE's injection system requires further research on rigorous durability and wear testing.

Review by Okokpujie et al. (2023, pp. 9–11) of different corrosion studies of ICE materials with various fuels and environments results that the immersion test with stainless steel, steel, iron and copper with jatropha biodiesel shows that copper has the highest and stainless-steel the lowest corrosion tendency. Review also shows that ethanol in ICE induced more corrosion in the piston, rings and valves than gasoline. Prosopis Juliflora biodiesel in ICE contributes ICE performance, reduces corrosion and emissions. Review shows that biodiesel in automotive engines, when added additives optimized properties of combustion and conducted minor damage in ICE.

3 Corrosion

Hänninen et al. (2022, p. 167–168). define corrosion as an oxidation process that degrades metals over time. Corrosion is electrochemical or chemical metal erosion caused by environmental factors. Corrosion occurs through an oxidation-reduction reaction. The embrittlement of metal due to stress is also counted as corrosion. Corrosion in metal materials causes economic harm, work safety risks and environmental degradation

Peda.net (2018) describes that in iron corrosion the oxygen from the air oxidizes the iron electrochemically. Iron and oxygen form a chemical pair, where iron is negatively charged, and oxygen is positively charged. In this reaction water acts as an electrolyte and conducts an electric current. If water contains sodium chloride (NaCl) or salt, it advances corrosion. Below is an example of iron corrosion (Formula 12 and Figure 1). Iron (Fe) together with oxygen and water forms a chemical reaction conducive to corrosion, where the final products are iron corrosion and hydroxide (OH^-).

$$2Fe(s) + O_2(g) + 2H_2O(l) \rightarrow 2Fe^{2+}(aq) + 4OH^-(aq) \qquad (12)$$

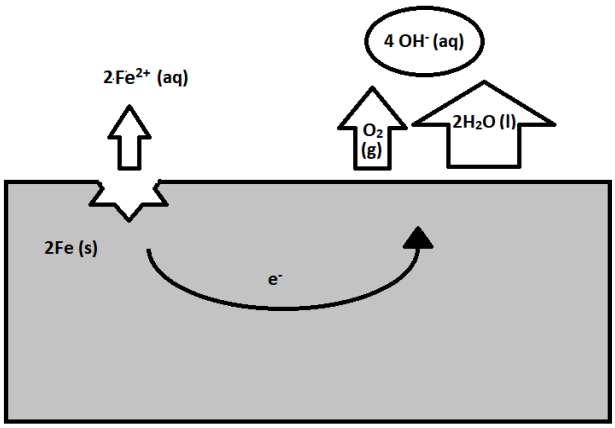

Figure 1. Corrosion of iron (adapted from Peda.net, 2018).

According to Hänninen et al. (2022, p. 169) corrosion reaction requires three factors: anode, cathode and electrolyte. If one of these factors is missing, corrosion will not occur. Oxygen, water, acidity or certain anions cause corrosion of metals, excluding more noble metals such as gold (Au) and platinum (Pt). In corrosion reaction less noble metal oxidizes and erodes. The oxidizing agent in the reaction is oxygen or water. In corrosion reaction metal transforms into metal ions and metal lattice becomes an ion lattice. Corrosion significantly weakens the structure of the metal.

3.1 Factors affecting the appearance of corrosion

Hänninen et al. (2022, pp. 167–168) describe that corrosion is caused by the tendency of metals to aim for the state of minimum energy. The environmental factors affecting the occurrence of corrosion are temperature, harmful chemicals and air humidity. Increase in temperature accelerates corrosion. According to Zafar et al. (2022, p. 3) the lifespan of the metal and its reduction is affected by surface breakage, which makes the material exposed to strain and stress. Together with the environmental factors like acidity and chemical reactions, the incidence of corrosion accelerates considerably and embrittles the metal structures. Factors affecting the occurrence of chemical corrosion are moisture, liquid, ionic solution, dry gases and microbes. Electrochemical corrosion is affected by micro-cell formation and electrolytes such as salt water.

Zafar et al. (2022, pp. 6, 9) state that corrosion of metals and their alloys is originated from chemical and electrochemical reactions together with the environmental factories. This occurs because of metals and their alloys strive for a stable chemical form. During this process, the metal weakens, losing its mechanical strength and elasticity. The incidence of corrosion can be prevented by various methods, such as using inhibitors and protective coating.

Hänninen et al. (2022, p. 148) clarified that the galvanic series of metals (Figure 2) explains the occurrence of oxidation between metals. The base metals in the figure are with the blue background, left from the hydrogen (H, the gray background). The noble

metals are in the figure with the yellow background, right from the hydrogen. Among the base metals, lithium (Li) has the greatest tendency to enter the cation state (Li^+), meaning it oxidizes most easily. Among the noble metals, gold has the least tendency to oxidize. Noble metals can be found in nature in metallic form and base metals are naturally compounds. If two metals meet one another, the more noble metal reduces and the less base metal oxidizes.

Figure 2. Galvanic series (adapted from Hänninen et al., 2022, p. 148).

3.2 Corrosion challenges in engine

Hoang et al. (2020, pp. 2923–2924, 2935–2938) describe that fuel passes through the ICE when it is used. The fuel travels from the tank through the entire fuel system: pumps, filters, the entire fuel line and injection system. The risk of corrosion increases everywhere the fuel moves. Corrosion causes many challenges in the ICE. If metal-contaminated fuel is used the risk of ICE failure increases considerably. The metal in the fuel can dissolve from the metal parts of the ICE or alternatively the fuel can already be contaminated with metal during the manufacturing process due to the raw materials.

Hänninen et al. (2022, p. 172) propose that the possibility of corrosion should be considered already in the ICE design stage by selection of materials and the design structures. In the ICE design, the galvanic series (Figure 2) of metals should be considered and joints of metals of different quality should be avoided. The homogeneity of the metal surface prevents corrosion.

According to Avtotachki (2022) corrosion can significantly affect the ICE in terms of lifespan, performance, various malfunctions and breakage. Corrosion embrittles the metal parts of the ICE. Corrosion effect can be seen, for example, in the weakness of structures. If the corrosion is in the ICE chamber, metal particles can cause the blockage

of the filters. Clogging in the filters can lead to engine failure in the worst-case scenario. The ICE running problems might be caused by particles in the fuel caused by corrosion.

Worldwide Fuel Charter (2009, pp. 8–10) profess that trace metal contamination in the fuel, for example, vanadium (V), sodium (Na), iron, silicon (Si), calcium (Ca), magnesium (Mg), aluminum, and nickel have a harmful effect on ICE fuel input system containing nozzles and valves and exhaust gas system. Catalyst deactivation can be caused by trace element contamination. In the combustion reaction of the ICE, trace metal particles can conduct ash formation. Blockage of filters and composition of deposits can be caused by ash formation. Vanadium and sodium can cause hot corrosion in the ICE. Alkaline metals, for example, sodium and potassium (K), can create challenges for emission aftertreatment systems. Sirviö et al. (2023, pp. 1, 8) discovered in their study on the properties of biodiesel the same challenges trace metal contamination in the biodiesel. According to the study, metals can speed up the oxidation reaction of fuel.

Oni et al. (2022, p. 7510) state that different alternative fuel qualities such as biodiesel also cause challenges in the ICE. The challenge of biodiesel is the ICE's cold start, which causes corrosion. This originates from the stiffening of ICE's motor oils due to the cold temperature, making them unable to protect the ICE as desired.

Mankonen (2014, pp. 13, 25–26) indicates that the characteristics of bio-oils, such as high density and low calorific value, create a challenge for fuel injection. These bio-oil characteristics also lead to very strong wear of materials, which occur in the fuel injection nozzle as corrosion and detrition. The ignition delay of bio-oil is caused by slow reaction kinetics, which affects the economic efficiency of the ICE. The use of bio-oil in an ICE requires modifications to the fuel injection system. Using bio-oil as fuel in an ICE requires blending it with ethanol or MeOH, for example. Bio-oil can cause damage to the combustion chamber and corrode the exhaust valves.

According to Avtotachki (2022) to extend the lifespan of the ICE and prevent damage caused by corrosion, regular maintenance should be performed and changes in the operation of the ICE should be considered. Repairing corrosion damages before major engine failure allows a long-term ICE. BG Suomi (n.d.) states that corrosion causes detrition in the engine and these influences moving parts in the ICE. The ICE must withstand corrosion during its lifespan, if the engine has been used according to the manufacturer's instructions. Factors primarily affecting the lifespan of the ICE are different types of fuel, motor oils, regular maintenance and corrosion inhibitors. Bruun (2022, p. 8) states that by adding corrosion inhibitors in the ICE is practice for preventing corrosion. Corrosion inhibitors form a protective layer on the surface of the metal. In the future, applying corrosion inhibitors in the ICE will increase (Oni et al., 2022, p. 7511).

3.3 Corrosion testing methods

The ASTM G1 – 03 standard, issued by the American Society for Testing and Materials, specifies the standard practice for preparing, cleaning and evaluating corrosion test specimen (ASTM International, 2017). Shehzad et al. (2021, pp. 3, 19) state that corrosion can be investigated with the immersion test and the electrochemical method. The immersion test is a more used analysis method in scientific research compared to the electrochemical method. The surface of the sample metal experienced from corrosion can be imaged with various surface description methods.

3.3.1 Immersion test

In the immersion test conducted by Ateeq et al. (2022, pp. 4–7), the preparation of the study starts by cutting metals into suitable pieces. In the immersion test a hole is drilled in the metal samples and then used for hanging metal samples into the fuel. The surface of the metal samples is sanded and polished using silicon carbide papers of different roughness classes. The pieces of metal sample are carefully cleaned with distilled water and dried. The sample metals are cleaned from grease with acetone. After preparing and cleaning, the metal samples are weighed separately and reported with accuracy of four

decimals. Next, the sample metals are immersed in the investigated fuel (Figure 3). After the time specified in the study, the metal samples are removed from the fuel. The metal samples are carefully cleaned again with acetone and weighed. Corrosion is observed as an altered, reduced weight of the metal samples. The initial weight and final weight are used to calculate the degree of corrosion using Formula 13, where *CR* is corrosion rate (µm/year) (ASTM International, 2017). Shehzad et al. (2021) describe similar procedure of conducting the immersion test.

$$CR = \frac{8{,}76 \cdot 10^7 \cdot \Delta m}{\rho \cdot A \cdot t} \tag{13}$$

CR = Corrosion Rate (µm/year)

Δm = mass loss in grams (g)

ρ = density (g/cm^3)

A = surface area (cm^2)

t = time of exposure (h)

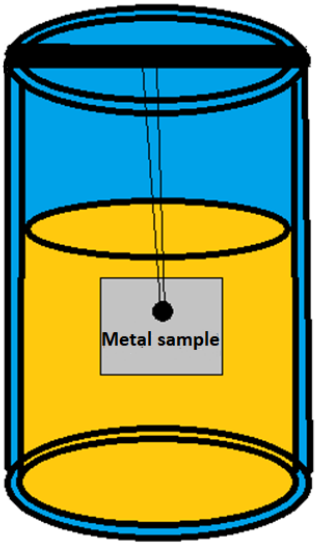

Figure 3. Immersion test: Sample metal in fuel (adapted from Shehzad et al., 2021, p. 3).

In the immersion test performed by Bruun (2022, pp. 11–12, 72), metal rods are cleaned and immersed in the tube containing biofuel. Tube containing the metal rods and biofuel are inserted in the mixer, which mixes the tubes through the immersion test. After the

time specified in the study, the metal rods are removed from the sample tubes. The metal is carefully cleaned with ultrasound using a mixture of toluene and 2-propanol. The biofuel solution used in corrosion testing is extracted and filtered through filter paper. The filtered biofuel solution corrosion is analyzed with a spectrophotometer. The spectrophotometer measures the absorption of wavelengths in the biofuel solution, which is used to determine its composition. The filtered biofuel solution is chemically changed into a form whose absorbance can be measured between 0.5 and 1. Metal dissolution in biofuel was investigated using an Inductively Coupled Plasma Optical Emission Spectroscopy (ICP-OES).

Bruun, (2022, p. 74) indicates the properties of the biofuel, for example the acid number, the amount of water and the combination of oils can be determined and measured in different ways. Shehzad et al. (2021, p. 32) state that the composition of the biofuel and corrosion rate results can be compared and conduct the conclusions about the corrosion properties caused by different biofuels. The immersion test as a corrosion analysis method can be varied in terms of time, temperature and the quality of fuels.

According to the Shehzad et al. (2021, p. 3) the immersion test duration is long, usually lasting several weeks. Longer exposure time in the fuel allows the sample metal to settle. The results obtained from the immersion test can be presented as a linear relationship between the degree of corrosion and time. The immersion test characterization techniques enable to find those metals which are prone to corrosion. In the immersion test, the colors of both the metal and the biofuel change, which helps to visually observe the formation of corrosion.

The Corrosion Rate results from the immersion test can be converted from mpy (mils per year) unit to µm/year using the Formula 14 (ASTM International, 2017).

$$X\ mpy = \frac{X \cdot (8{,}76 \cdot 10^{7})}{(3{,}45 \cdot 10^{6})} \quad (14)$$

X = Corrosion Rate in mpy unit

3.3.2 Electro-Chemical method

According to Shehzad et al. (2021, p. 3) measurement of metal corrosion resistance using an electro-chemical method is based on oxidation and reduction reactions. The electro-chemical method of corrosion is based on the transfer of electrons and electric current, so the amount of corrosion can be measured and calculated using electricity. Ahn et al. (2002, pp. 319–321) describe similar procedure of conducting the electro-chemical method.

Shehzad et al. (2021, p. 3) clarified that when using electrochemical method, the corrosion resistance of the metal itself is not tested under the influence of the fuel. This is the reason for the immersion test being the most suitable method to study the corrosion durability caused by fuels in the metal. The electrochemical method is a relatively fast way to study the corrosion resistance of a metal, with the analysis method taking only a few hours.

3.3.3 Characterization techniques of the corroded surface

Shehzad et al. (2021, p. 19) suggest that corrosion can be observed and studied using various surface characterization techniques. The method used to cause corrosion in metal samples, the immersion test or the electrochemical method, is selected. The damage caused by corrosion in the sample metals can be examined using characterization techniques such as various microscopes and X-rays. Characterization techniques of corroded surface are SEM, Energy Dispersive Spectroscope (EDS), Atomic Absorption Spectrometry (AAS), Optical Microscope (OM), X-ray diffraction (XRD) and X-ray Photoelectron Spectroscope (XPS).

4 Materials and methods

This chapter is divided into materials, methods and quality assurance sections. The material section reviews fuels and properties of the CS samples used in the immersion tests. The method section describes in detail the implementation of the immersion tests and the laboratory analysis methods for fuels and the CS samples. For this study, the immersion test procedure was developed for the University of Vaasa's Fuel laboratory. The immersion test method was developed in sectors: the CS samples size, sample container and sample attachment method, preparation of the fuel blend, temperature effect on the immersion tests results and SEM images. This study was executed in the way the immersion test procedure was developed. The last section describes the research's quality assurance of the methods.

4.1 Materials

The materials used in this study were MeOH, RD, blend and LFO fuels. The chapter describes the fuel blend preparation method. The second section of this chapter describes detailed properties of the CS samples.

4.1.1 Fuels

The RD, MeOH and LFO fuels used in the immersion tests were ready-made by the manufacturers. The RD and LFO were supplied by Neste Corporation, Finland, and were intentionally unadditivised. More detailed information about fuel manufacturers and other chemicals used in this study can be seen in Table 1.

Table 1. Information about the chemicals used in the immersion tests.

Chemicals	**Kinematic Viscosity** [mm^2/s]	**Density** [kg/m^3]	**Manufacturer**
RD without additives: Neste Renewable Diesel	3.05	781	Neste Corporation
Methanol for analysis (MeOH)	0.56	796	Emsure®, Supelco
Fossil Diesel (LFO)	3.41	841	Neste Corporation
1-octanol for synthesis	-	-	Merck, Sigma-Aldrich
2-Propanol for analysis (for purification of the CS samples)	-	-	Emsure®, Supelco

The immersion test was executed at two different periods of time due to the different desired temperatures in the heating cabinet. Therefore, the fuel blend of RD, MeOH and 1-octanol were prepared at two different times. The blend of RD and MeOH needed 1-octanol as an adhesive so that the fuels become miscible with each other.

The fuel blend was prepared both times in the same practice with retain to the amount of RD and MeOH. The amount of RD in the fuel blend was 242 ml and MeOH was 58 ml. The amount of 1-octanol was 51.6 ml in the first immersion test at temperature of 23 °C and 54.6 ml in the second time at temperature of 40 °C (Table 2). The environmental temperature influences the amount of 1-octanol required in the fuel blend. 150 ml of the fuel blend was measured and bottled for the immersion test. The rest of the fuel blend was used in fuel content analyses. Based on LHV of the fuel blend content, the final energy ratio was calculated (Table 2). The final energy ratio of the fuel blend at temperature of 23 °C was distributed as follows RD 78 %, MeOH 8 % and 1-octanol 14 %. The final energy ratio of the fuel blend at temperature of 40 °C was distributed as follows RD 77 %, MeOH 8 % and 1-octanol 15 %.

Table 2. Fuel blend volumes and the final energy ratio.

	LHV	Fuel blend at 23 °C	The final energy ratio at 23 °C	Fuel blend at 40 °C	The final energy ratio at 40 °C
RD	44.0 MJ/kg	242 ml	78 %	242 ml	77 %
MeOH	20.0 MJ/kg	58 ml	8 %	58 ml	8 %
1-octanol	37.6 MJ/kg	51.6 ml	14 %	54.6 ml	15 %

Initially, the fuel blend at 23°C was colorless. After exposure to air, it became cloudy but later returned to a clear state. In contrast, the fuel blend at 40°C remained colorless throughout the process. Figure 4 shows the comparison with the different fuel blends. In the figures labels MeOH10 means the fuel blend.

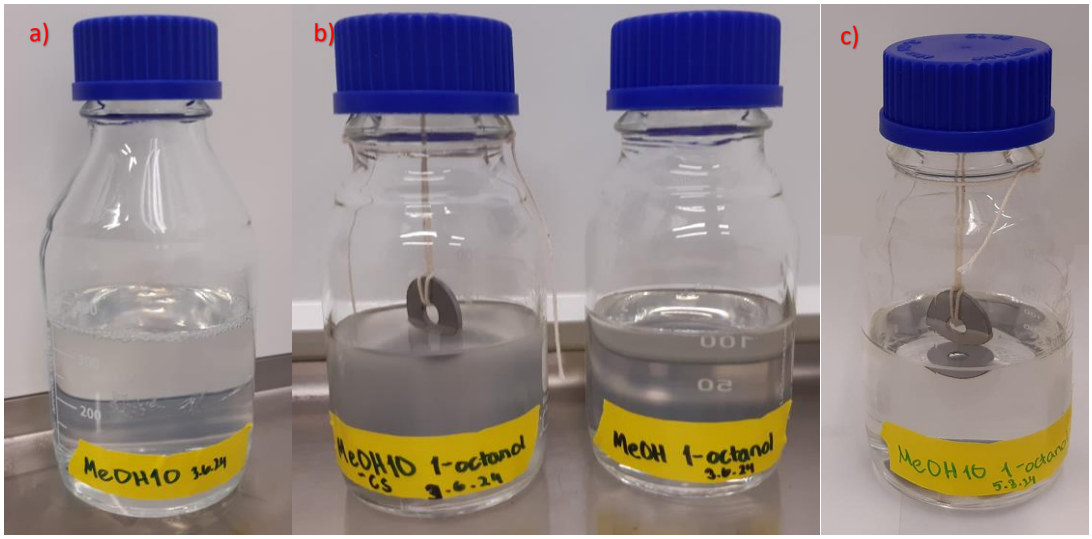

Figure 4. Fuel blend comparison. In the figure labels MeOH10 means the fuel blend. a) After making the fuel blend for the immersion test at 23 °C. b) After exposure to air, the fuel blend became cloudy. c) Colorless fuel blend for the immersion test at 40 °C.

4.1.2 Carbon Steel

Niemi and Ovaska (n.d., pp. 26, 31) confirm that CS is a metal alloy, and it contains iron, carbon and other chemical elements. At least grade E295 CS is used as the material of the lightly loaded ICE connecting rod. The crankshaft, counterweights and bearing points of high-speed diesel engines can be made of high-quality CS, but they are commonly made of hardened steel. Bejinariu et al. (2020, p. 1) state that CS has low corrosion

resistance compared to many other metals. Corrosion resistance affects the mechanical properties and durability of CS negatively. The corrosion resistance of the CS can be increased by adding a corrosion protection layer on the surface of the metal.

The CS used in this study contains iron, carbon, silicon, manganese (Mn), phosphor (P), sulfur, chrome (Cr), aluminum, molybdenum (Mo) and nickel. The accurate content of the CS used in this study is shown in Table 3.

Table 3. The content of the CS used in this study (Ampko Oy, 2017).

Trace metals	**Abbreviation**	**Rate**
Iron	Fe	97.995 %
Carbon	C	0.743 %
Silicon	Si	0.256 %
Manganese	Mn	0.670 %
Phosphor	P	0.014 %
Sulfur	S	0.023 %
Chrome	Cr	0.216 %
Aluminum	Al	0.010 %
Molybdenum	Mo	0.026 %
Nickel	Ni	0.047 %

The CS samples were commissioned with certain precisely defined properties. Surface area and volume were calculated from the known size of the CS samples.

- Shape: Round
- Size:
    - Diameter 25 mm
    - Hole diameter 8 mm
    - Thick 2 mm
- Uncoated
- No bending
- Surface area [*A*]: 10.89 cm^2
- Volume [*V*]: 0.88 cm^3

4.2 Methods

This research was divided into two parts. The immersion test of the CS samples at two different temperatures of 23 °C and 40 °C.

4.2.1 Immersion test

The CS samples were prepared before the immersion tests. Preparation holds purification of the CS samples with 2-propanol and lint-free tissue to remove grease and other contaminations from the samples surface. After purification the CS samples weight were measured with five digits. After weighing the samples were purified with 2-propanol again.

After cleaning and weighing, the CS samples were attached to RD, MeOH, blend and LFO fuel sample containers. Lint-free cotton thread was used for fastening the CS samples. One of the CS samples was immersed into the bottom of the sample containers and the other was fastened to hang on the middle of fuel and air interface. In the first immersion test, the temperature of the heating cabinet was adjusted to 23 °C and in the second immersion test to 40 °C. Figure 5 shows fuel samples preparation before the heating cabinet. In the figures labels HVO means RD. The duration of the first immersion test at temperature of 23 °C was 307 hours [h]. The duration of the second immersion test at temperature of 40 °C was 311 h.

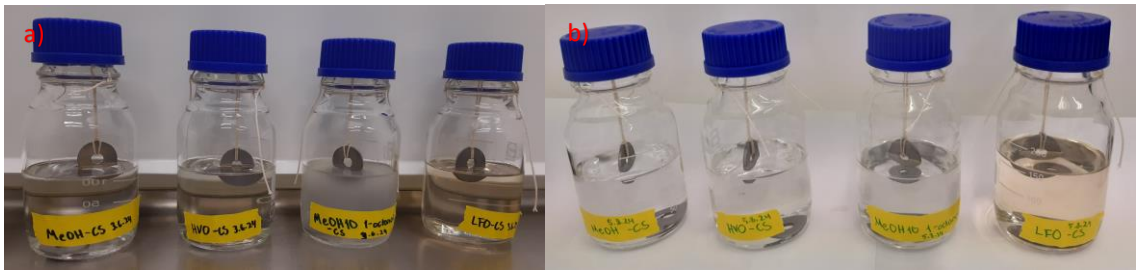

Figure 5. Fuels samples preparation before the heating cabinet. In the figure labels MeOH10 means the fuel blend and HVO means RD. a) Fuels with the CS samples in the immersion test at temperature of 23 °C. b) Fuels with the CS samples in the immersion test at temperature of 40 °C.

After the immersion test, the CS samples were taken out of the fuel and cleaned carefully with 2-propanol and a lint-free tissue. Visual observation of the corrosion was made with the CS samples and fuel samples. The CS samples were weighed again. The CS samples that fastened to hang in the middle of fuel and air interface, were marked from the point of the cotton string with black marker. The purpose of the mark was to determine the position of the CS sample in the fuel. After cleaning, visual observation, weighing and marking the CS samples, SEM images were taken (Figure 6).

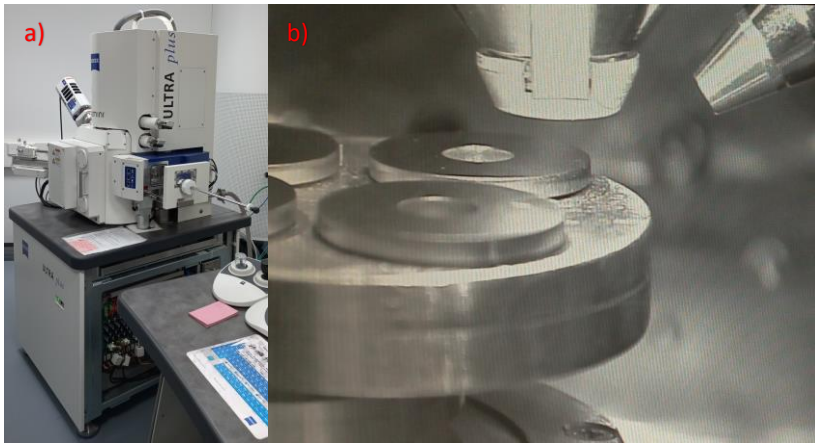

Figure 6. a) Scanning electron microscope. b) The sample stage with the CS samples in the chamber.

Density, kinematic viscosity and distillation were analyzed before and after the immersion tests. The trace metal concentration measurements were analyzed before and after the immersion tests. The measurements were made twice. The presented

results were arithmetic mean (Formula 15) calculated from the measurements to ensure quality assurance. Trace metals concentration measurements were performed with two different ICP-OES analyzers. RD and LFO fuel samples were analyzed with one analyzer and MeOH and fuel blend samples with the other.

4.2.2 Laboratory analysis methods of the fuels

The following analysis was performed from the MeOH, RD, blend and LFO fuels before and after the immersion test: kinematic viscosity, density, distillation and the measurements of the trace metal concentrations.

Kinematic viscosity and density were measured with the same analyzer Anton Paar Stabinger SVM 3000 viscometer. Kinematic viscosity was measured at 40 °C and density at 15 °C temperature. Anton Paar (n.d., pp. 2, 4) verifies that the Anton Paar Stabinger SVM 3000 viscometer device determines dynamic viscosity using the rotor speed. The density of the fuel was determined in the measuring chamber. The kinematic viscosity of the fuel was determined based on the previous two measurements dynamic viscosity and density results. Anton Paar Stabinger SVM 3000 viscometer measurements were compatible with standard ASTM D7042 as well as measurement of ASTM D2270 and ISO 2909 viscosity index.

Distillation of fuels were measured with PAC ISL OptiPMD analyzer. PAC (2019, pp. 1–2) describes that the distillation method was based on vapor, liquid temperature variations and pressure measurements at atmospheric pressure. PAC ISL OptiPMD analyzer was compatible with ASTM S7345, EN 17306 and IP 596 standards.

Measurements of the trace metal concentrations in fuels were measured with an ICP-OES analyzer. Wang-Alho et al. (2024, p. 4) state that the purpose of ICP-OES trace metal concentrations measurements was to measure the elements dissolved in the fuels from the CS metal samples. The ICP-OES analyzer operates by comparing known trace metal concentrations emission to the intensity emitted by wavelength of light. The ICP-OES

analyzer estimates the samples trace metals and their concentration comparing the result of known trace metal concentrations.

The trace metal concentrations measurements of LFO and RD fuels were analyzed with PerkinElmer Optima 700 DV ICP-OES analyzer. MeOH and blend fuels were measured with PerkinElmer Avio 500 ICP-OES analyzer. For RD and LFO fuel samples, the concentrations of the trace metals aluminum, copper, iron, manganese, silicon, vanadium, zinc and lead (Pb) in LFO and RD fuels were determined by ICP-OES analyzer. In addition to the previous trace metal, phosphorus, sulfur, chromium, molybdenum and nickel concentrations in MeOH and fuel blend were determined. RD and LFO fuel samples were diluted with kerosene in a weight ratio of 1:1. MeOH and fuel blend samples were prepared by acid digestion before the trace metal concentrations measurements. Digestion occurs by the aid of nitric acid in a microwave oven (MARS 6 iWave by CEM). The purpose of digestion is to break down all inorganic particles into sizes smaller than 8 µm and annihilate the remaining organic mass. The MeOH and blend fuel samples completely dissolved during wet combustion. MeOH and blend fuel samples were diluted and analyzed. The ICP-OES analyses in both analyzers were performed by in-house methods, according to the device manufacturer's instructions and following the standard SFS-EN 16576. Standard SFS-EN 16576 specifies how to determine manganese and iron concentration from diesel fuel using the ICP-OES analysis method (Finnish Standards Association, 2014).

4.2.3 Laboratory analysis methods of the carbon steel

The CS samples analysis methods in this study were visual observation of corrosion, weighing, calculating corrosion rate from the results and SEM images.

Visual observation of corrosion was made after both immersion tests at temperature of 23 °C and 40 °C in identical practice. The visual observation aimed to observe the visible corrosion of the CS samples caused by the fuels. The samples were compared to an

unused CS sample. Tactile inspection was used to observe the sharp points of the CS plates. Observations were scribed and compared to SEM image results.

The CS samples were weighed with Mettler Toledo XS205 DualRange scale. After cleaning with 2-propanol and lint-free tissue the CS samples were weighed before and after the immersion tests at temperatures of 23 °C and 40 °C. Measurements were recorded to five decimal places. Corrosion rate was calculated from the weight loss results.

SEM images from the CS samples were made with Zeiss Ultra plus FESEM microscope. Heikkinen and Tanskanen (2022, pp. 2–3) profess that the operation of the SEM is based on a high intensity electronic current focused on the sample. The electrons concentrated in the sample are affected by the atoms in the sample. The secondary electron detector receives the electron beam. The use of the SEM requires a vacuum, therefore the samples must be vacuum-resistant and electrically conductive.

4.3 Quality assurance of the methods

According to the manufacturer, the MMM Group Venticell Eco line heating cabinet maintains a temperature accuracy of ±0.4 °C for temperatures above 50 °C (MMM Group, 2012, p. 16). During the experiment, the temperature of the heating cabinet was first adjusted to a temperature of 23 °C. During this experiment, the heating cabinet temperature remained almost the same, rising up to 24 °C maximum. In the second part of the experiment, the temperature of the heating cabinet was set to 40 °C. In this experiment the temperature remained very close to the set temperature and the range given by the user manual. The temperature remained between 39.6-40.4 °C.

According to the manufacturer of the analytical scale Mettler Toledo XS205 DualRange used in the study, the measurements error Sensitivity offset was 0.00015 % times the mass of the sample (Mettler Toledo, 2013, p. 28). The CS metal samples used in this study

error sensitivity offset was ±0.001032-0.001034 grams (g). According to the validation measurement with Mettler Toledo scale relative standard deviation (*RSD*) was under 1 %.

The laboratory analysis methods used in the study were performed twice for each sample. The measurement results presented in the study were the arithmetic mean of these two values (Formula 15) (Mäkelä et al., 2020, p. 84). The measurement methods have been validated, and the standard deviation of the sample has been determined for the methods (Formula 16) (Mäkelä et al., 2020, p. 85). The relative standard deviation can be determined using the standard deviation (Formula 17) (Jaarinen & Niiranen, 2005, p. 32).

$$\bar{x} = \frac{\sum_{i=1}^{n} x_i}{n}. \quad (15)$$

$\overline{x} =$ Arithmetic Mean

$n =$ Number of the Observations

$x_i =$ Individual Observation Value

$$s = \sqrt{\frac{1}{n-1}\sum_{i=1}^{n}(x_i - \overline{x})^2}. \quad (16)$$

$s =$ Sample Standard Deviation

$$RSD = \frac{s}{\overline{x}} \times 100\ \%. \quad (17)$$

$RSD =$ Relative Standard Deviation

Based on validation measurements, relative standard deviation for different measurement methods were:

- Distillon PAC ISL OptiPMD: *RSD* < 1 %
- Density Anton Paar Stabinger SVM 3000 viscometer: *RSD* < 1 %
- Kinematic viscosity Anton Paar Stabinger SVM 3000 viscometer: *RSD* < 1 %

ICP-OES relative standard deviation was not calculated. ICP-OES analyzed results quality control was performed with analyzing samples two times. ICP-OES analyzers have internal standard quality control. The control sample which has known concentration values was also used for quality assurance of the method.

Two unused CS samples were selected as controls to ensure the quality of the SEM images. Neat and scruffy CS samples were chosen as a control, which were cleaned with 2-propanol and lint-free tissue before taking SEM images.

5 Results

This chapter presents the results of the immersion test at temperature of 23 °C and 40 °C. During the immersion test, MeOH and fuel blend had evaporated from the container containing CS samples (Figure 7). At the beginning of the immersion tests, 150 ml of fuels were measured in the sample containers. The exact volume of the fuels that evaporate was not measured. The immersion test at temperature of 23 °C, MeOH fuel evaporated about 10 ml, which is about 7% of the original sample amount. The immersion test at 23 °C, the blend evaporated about 5 ml, which is about 3% of the original sample amount. The immersion test at 40 °C, MeOH fuel evaporated about 25 ml, which is about 17% of the original sample amount. The immersion test at 40 °C, the blend evaporated about 10 ml, which is about 7% of the original sample amount. In the RD and LFO fuels, the fastening cotton threads were wet after both immersion tests. With MeOH and fuel blend with the CS samples the fastening cotton threads were dry.

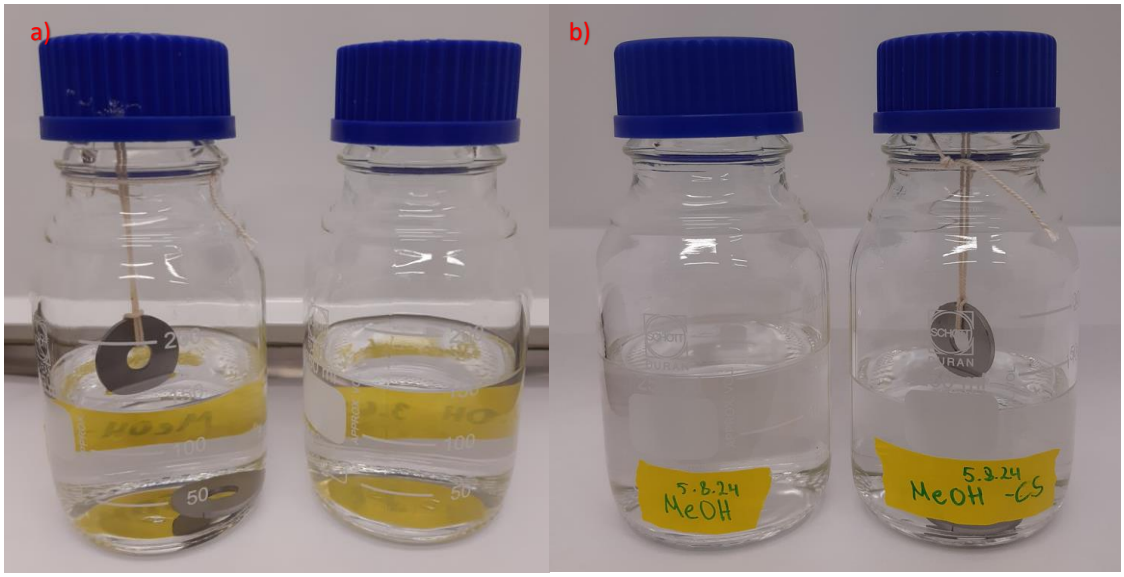

Figure 7. Evaporated MeOH sample after the immersion test. Comparison between fuel samples with the CS samples and without. a) After the immersion test at temperature of 23 °C. b) After the immersion test at temperature of 40 °C.

5.1 Visual observation of the corrosion

The visual observation detects that the CS samples on the other edge were sharper than the other. Tarnish was visually detected on the sharper edge of each CS sample during both immersion tests. The CS samples had prominent lines at the outside and inside edge. During both immersion tests, tarnish was formed in the edge's prominence line. During both immersion tests with MeOH fuel, a visual light-colored mark was left on the metal surface from the cotton thread of the hanging CS sample. The immersion test was conducted at temperature of 23 °C, the fuel blend caused tarnish spots to the inner surface edge of the hole in the CS sample, which was below the surface of the fuel solution (Figure 8).

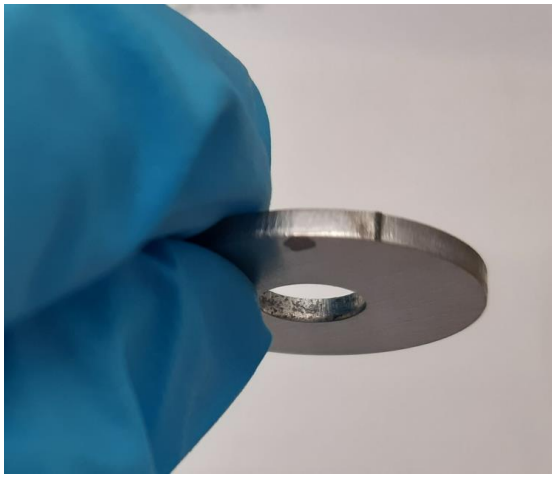

Figure 8. The immersion test at temperature of 23 °C: Hanging CS sample from fuel blend with visual tarnish spots on edge of the sample hole.

5.2 The carbon steel samples weights and corrosion rate

The CS samples were weighed before and after the immersion test. The CS samples weight loss after the immersion test is shown in Table 4. Weight loss was calculated from the weight before the immersion test minus sample weight after the immersion test.

Table 4. The CS samples' weight loss after the immersion test. (1. CS sample on the bottom of the fuel container and 2. hanging CS sample between the fuel and air interface.)

	Weight loss [g] after the immersion test (23 °C)	**Weight loss [g] after the immersion test (40 °C)**
1. RD	0.00001	0.00001
2. RD	0.00001	0.00003
1. MeOH	0.00000	0.00004
2. MeOH	0.00002	0.00036
1. Blend	0.00004	0.00005
2. Blend	0.00008	0.00014
1. LFO	0.00001	0.00005
2. LFO	0.00000	0.00000

From the weighing results, after both immersion tests, the weights of the CS samples decreased little or not at all. The weight descent with different the CS samples was between 0 to 0.00036 g. The largest weight descent occurred in the immersion test performed at temperature of 40 °C for the CS sample hanging between fuel and air interface, when the fuel was MeOH. The weight loss of this sample was 0.00036 g. The immersion test was performed at temperature of 23 °C on the CS sample hanging between fuel and air interface, with the fuel being blend, the weight loss of this sample was 0.00008 g. The immersion test was performed at temperature of 40 °C for the CS sample hanging between fuel and air interface, when the fuel was blend, the weight loss of this sample was 0.00014 g.

Corrosion rates were calculated from the calculated weight losses from immersion tests. Corrosion rates were calculated by Formula 13. Results are shown in Table 5. Surface area and volume of the CS samples were in chapter 4.1.2 Carbon Steel. An arithmetic mean (Formula 15) was calculated from the measured weights of the CS samples, which were used to calculate the density. The duration of the first immersion test at temperature of 23 °C was 307 hours (h). The duration of the second immersion test at temperature of 40 °C was 311 h.

Table 5. Corrosion rate [µm/year].

	CR [µm/year] immersion test (23 °C)	*CR* [µm/year] immersion test (40 °C)
1. RD	0.03	0.03
2. RD	0.03	0.10
1. MeOH	0	0.13
2. MeOH	0.07	1.19
1. Blend	0.13	0.17
2. Blend	0.27	0.46
1. LFO	0.03	0.17
2. LFO	0	0

The calculated corrosion rates for all the CS samples were between 0 to 1.19 µm/year. The highest corrosion rate occurred in the immersion test performed at temperature of 40 °C for the CS sample hanging between fuel and air interface, when the fuel was MeOH, the corrosion rate was 1.19 µm/year.

5.3 Kinematic Viscosity

Kinematic viscosity of the fuels was measured with the analyzer Anton Paar Stabinger SVM 3000 viscometer at temperature of 40 °C. Results are shown in Table 6. The kinematic viscosity analysis was done twice for verification and quality control. Results in Table 6 were the calculated arithmetic mean of the analysis results (Formula 15). In Table 6, fuels are divided into two, control fuel and the fuel with the CS samples.

The kinematic viscosity of the RD fuels varied between 3.05-3.06 mm^2/s before and after both immersion tests. RD fuels meet the requirements of the SFS-EN 15940 standard in terms of kinematic viscosity. The kinematic viscosity of the MeOH fuels varied between 0.55-0.57 mm^2/s before and after both immersion tests. MeOH fuels do not meet the requirements of standard SFS-EN 590 regarding kinematic viscosity. The kinematic viscosity of fuel blend varied between 2.40-3.08 mm^2/s before and after both immersion tests. Fuel blends meet the requirements of the SFS-EN 15940 standard in terms of

kinematic viscosity. The kinematic viscosity of the LFO fuels varied between 3.40-3.42 mm^2/s before and after both immersion tests. LFO meets the requirements of the SFS-EN 590 standard in terms of kinematic viscosity.

Table 6. Kinematic viscosity results before and after the immersion tests.

Kinematic viscosity measured at 40 °C temperature RSD < 1 %					
Fuel	*Before the immersion test at temperature of 23 °C [mm^2/s]*	*After the immersion test at temperature of 23 °C [mm^2/s]*	*Before the immersion test at temperature of 40 °C [mm^2/s]*	*After the immersion test at temperature of 40 °C [mm^2/s]*	***Standards*** (see Finnish Standards Association, 2023; Finnish Standards Association, 2017).
RD	3.05	3.05	3.05	3.05	***EN 15940*** *[mm^2/s]* 2.000-4.500
RD-CS	3.05	3.05	3.05	3.06	
MeOH	0.57	0.57	0.55	0.56	***EN 590*** *[mm^2/s]* 2.000-4.500
MeOH-CS	0.57	0.56	0.55	0.57	
Blend	2.43	2.64	2.52	2.40	***EN 15940*** *[mm^2/s]* 2.000-4.000
Blend-CS	2.43	2.64	2.52	3.08	
LFO	3.40	3.41	3.41	3.41	***EN 590*** *[mm^2/s]* 2.000-4.500
LFO-CS	3.40	3.40	3.41	3.42	

5.4 Density

Fuels densities were measured with the analyzer Anton Paar Stabinger SVM 3000 viscometer at temperature of 15 °C. Results are shown in Table 7. The density analyzes has been done twice for verification and quality control. Results in Table 7 are the calculated arithmetic mean from the analyzed results (Formula 15). In Table 7, fuels are divided in two, control fuel and fuel with the CS samples.

The density of the RD fuels was 781 kg/m^3 before and after both immersion tests. RD fuels meet the requirements of the SFS-EN 15940 standard in terms of density. The density of the MeOH fuels varied between 796-798 kg/m^3 before and after both immersion tests. MeOH fuels do not meet the requirements of the standard SFS-EN 590 regarding density. The density of fuels blend varied between 788-789 kg/m^3 before and

after both immersion tests. Fuels blend meets the requirements of the SFS-EN 15940 standard in terms of density. The density of the LFO fuels varied between 841-842 kg/m^3 before and after both immersion tests. LFO meets the requirements of the SFS-EN 590 standard in terms of density.

Table 7. Density results before and after the immersion tests.

Density measured at 15 °C temperature RSD < 1 %					
Fuel	*Before the immersion test at temperature of 23 °C [kg/m^3]*	*After the immersion test at temperature of 23 °C [kg/m^3]*	*Before the immersion test at temperature of 40 °C [kg/m^3]*	*After the immersion test at temperature of 40 °C [kg/m^3]*	***Standard*** (see Finnish Standards Association, 2023; Finnish Standards Association, 2017).
RD	781	781	781	781	***EN 15940*** *[kg/m^3]* 780-810
RD-CS	781	781	781	781	
MeOH	796	796	797	796	***EN 590*** *[kg/m^3]* 820.0-845.0
MeOH-CS	796	798	797	798	
Blend	789	789	788	788	***EN 15940*** *[kg/m^3]* 780-810
Blend-CS	789	789	788	789	
LFO	841	841	841	842	***EN 590*** *[kg/m^3]* 820.0-845.0
LFO-CS	841	841	841	841	

5.5 Distillation

Fuels distillations were measured with the analyzer PAC ISL OptiPMD. Results are shown in Table 8. The distillation analyzes have been done twice for verification and quality control. Results in Table 8 were the calculated arithmetic mean (Formula 15). The distillation method did not allow the measurement for the fuel blend, due to the temperature limitations determined by the analyzer, meaning RD, MeOH and 1-octanol have extremely different distillation temperature properties.

The distillation of the RD fuels initial boiling point (IBP) varied between 220.1-223.2 °C and final boiling point (FBP) varied between 308.4-313.0 °C before and after both immersion tests. The distillation of the MeOH fuels IBP varied between 64.7-65.7 °C and FBP varied between 72.7-77.3 °C before and after both immersion tests. The distillation

of the LFO fuels IBP varied between 195.9-199.1 °C and FBP varied between 345.6-347.5 °C before and after both immersion tests.

Table 8. Distillation results before and after the immersion tests.

Distillation: Initial Boiling Point and Final Boiling Point, RSD < 1 %								
Fuel	*Before the immersion test at temperature of 23 °C [°C]*		*After the immersion test at temperature of 23 °C [°C]*		*Before the immersion test at temperature of 40 °C [°C]*		*After the immersion test at temperature of 40 °C [°C]*	
	IBP	**FBP**	**IBP**	**FBP**	**IBP**	**FBP**	**IBP**	**FBP**
RD	222.8	308.4	220.1	310.8	221.3	310.1	220.9	313.0
RD-CS	222.8	308.4	220.6	311.5	221.3	310.1	223.2	311.3
MeOH	65.5	74.9	65.0	72.7	64.7	73.7	64.8	73.9
MeOH-CS	65.5	74.9	65.2	73.9	64.7	73.7	65.7	77.3
Blend	n/a	n/a	n/a	n/a	n/a	n/a	n/a	n/a
Blend-CS	n/a	n/a	n/a	n/a	n/a	n/a	n/a	n/a
LFO	197.4	346.3	195.9	346.3	197.6	345.6	198.2	347.5
LFO-CS	197.4	346.3	197.4	346.5	197.6	345.6	199.1	347.4

n/a = not analyzed

Distillation curves can be seen in Figures 9-12. Comparing the distillation curves of RD fuels before and after the immersion tests at 23 °C and 40 °C, the IBP and FBP temperatures are convergent and distillation curves profiles are similar. Comparing the distillation curves of MeOH fuels before and after the immersion tests at 23 °C and 40 °C, the IBP and FBP temperatures are convergent and distillation curves profiles are similar. Comparing the distillation curves of LFO fuels before and after the immersion tests at 23 °C and 40 °C, the IBP and FBP temperatures are convergent and distillation curves profiles are similar.

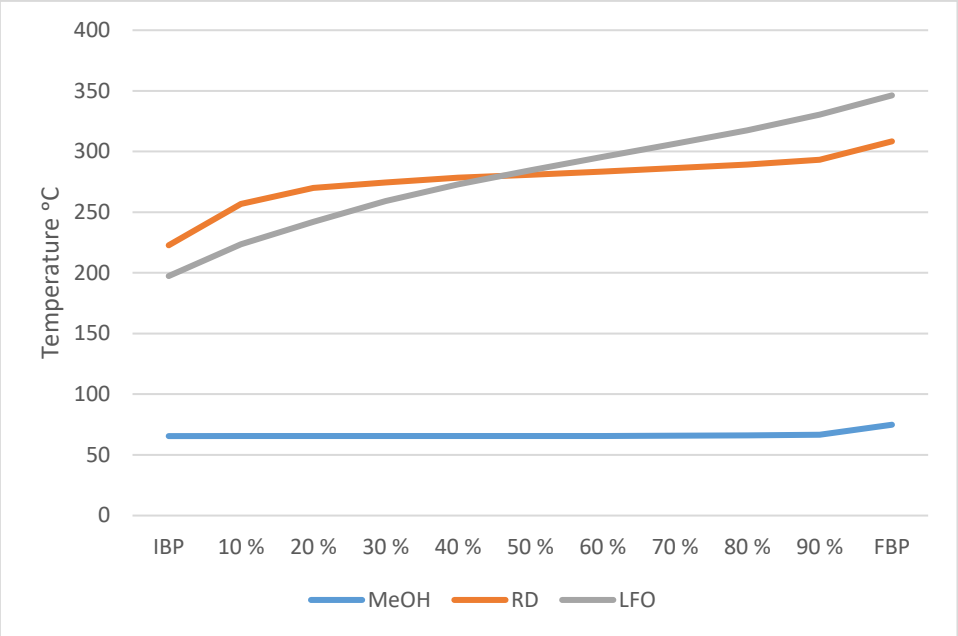

Figure 9. Distillation curves before the immersion test at temperature of 23 °C.

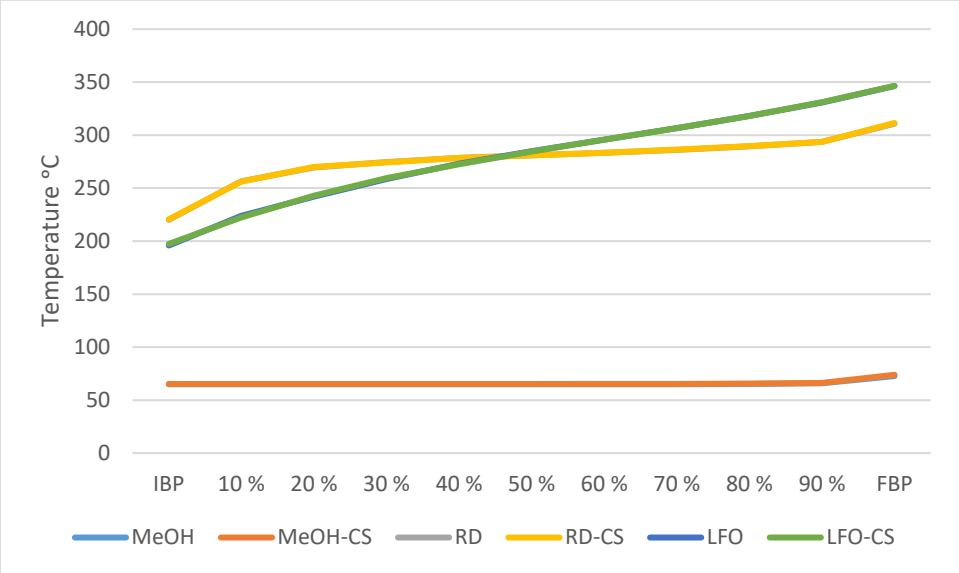

Figure 10. Distillation curves after the immersion test at temperature of 23 °C.

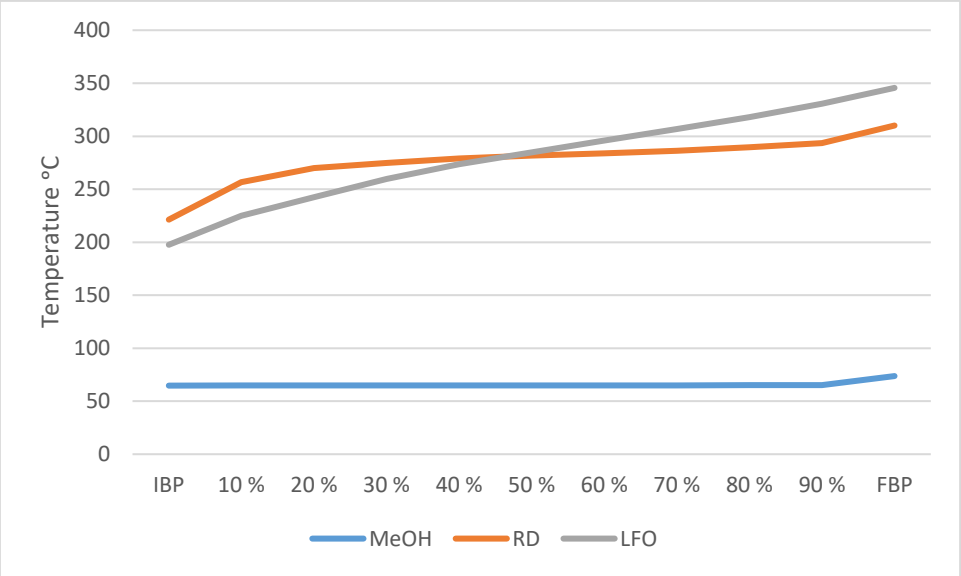

Figure 11. Distillation curves before the immersion test at temperature of 40 °C.

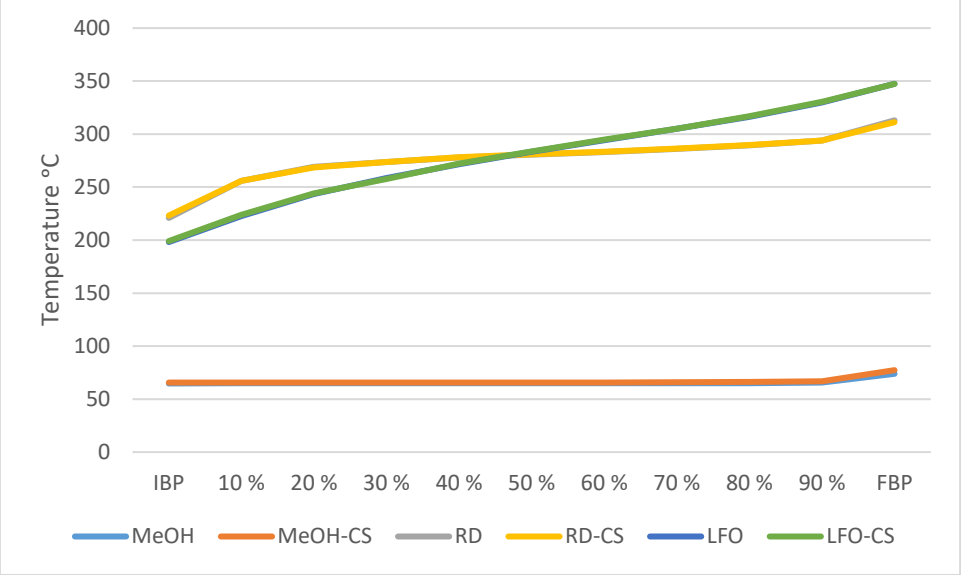

Figure 12. Distillation curves after the immersion test at temperature of 40 °C.

Standards SFS-EN 590 and SFS-EN 15940 have limitations for fuels distillation properties, what are presented in Table 9 and 10. RD fuel meets the SFS-EN 15940 standard limitations for fuels distillation properties (Table 9). The distillation curve of MeOH fuels does not meet the limits according to the standard SFS-EN 590. LFO fuel meets the SFS-EN 590 standard limitations for fuels distillation properties (Table 10).

Table 9. Distillation properties for RD compared to Standard SFS-EN 15940.

Distillation	**SFS-EN 15940** (Finnish Standards Association, 2023).	**RD**	**RD**	**RD -CS**	**RD**	**RD**	**RD -CS**
		Before 23 °C	**After 23 °C**	**After 23 °C**	**Before 40 °C**	**After 40 °C**	**After 40 °C**
% recovery at 250 °C [vol. %]	max. 65	8.0	8.3	8.3	8.1	8.3	8.2
% recovery at 350 °C [vol. %]	min. 85	100	100	100	100	100	100
95% recovery at [°C]	max. 360	301	302	303	302	303	303

Table 10. Distillation properties for LFO compared to Standards SFS-EN 590.

Distillation	**SFS-EN 590** (Finnish Standards Association, 2017).	**LFO**	**LFO**	**LFO -CS**	**LFO**	**LFO**	**LFO -CS**
		Before 23 °C	**After 23 °C**	**After 23 °C**	**Before 40 °C**	**After 40 °C**	**After 40 °C**
% recovery at 250 °C [vol. %]	max. 65	24.7	24.8	24.3	24.4	24.5	24.4
% recovery at 350 °C [vol. %]	min. 85	100	100	100	100	100	100
95% recovery at [°C]	max. 360	338	339	339	338	339	339

5.6 Measurement of the trace metal concentrations

The results of the fuels' trace metal concentrations analyses are presented in Table 11.

Table 11. Results of the trace metal concentration analyses of all fuel samples.

Trace metal concentrations	*Before (B) and after (A) the immersion test temperature 23 ºC ppm [mg/kg]*				*Before and after the immersion test temperature 40 ºC ppm [mg/kg]*			
	RD -CS B & A	**MeOH -CS** B & A	**MeOH 10 -CS** A	**LFO -CS** B & A	**RD -CS** B & A	**MeOH -CS** B & A	**MeOH 10 -CS** A	**LFO -CS** B & A
Al	<1	<1	<1	<1	<1	<1	<1	<1
Cu	<1	<1	<1	<1	<1	<1	<1	<1
Fe	<1	<1	<1	<1	<1	<1	<1	<1
Mn	<1	<2	<2	<1	<1	<2	<2	<1
Si	<1	<1	<1	<1	<1	<1	<1	<1
V	<1	<1	<1	<1	<1	<1	<1	<1
Zn	<1	<1	<1	<1	<1	<1	<1	<1
Pb	<1	<4	<4	<1	<1	<4	<4	<1
P	n/a	<4	<4	n/a	n/a	<4	<4	n/a
S	n/a	<4	<4	n/a	n/a	<4	<4	n/a
Cr	n/a	<1	<1	n/a	n/a	<1	<1	n/a
Mo	n/a	<1	<1	n/a	n/a	<1	<1	n/a
Ni	n/a	<1	<1	n/a	n/a	<1	<1	n/a

n/a = not analyzed

Trace metal concentrations for aluminum, copper, iron, manganese, vanadium, zinc and lead in the MeOH and RD used in the fuel blend are below 1 ppm concentration and below 500 ppm water content according to the manufacturer. The results of trace metal concentrations analysis were the same before and after both immersion tests. Trace metal concentration results of RD, MeOH, blend and LFO fuels were under one part per million (ppm) with aluminum, copper, iron, silicon, vanadium and zinc. RD and LFO fuels trace metal concentration results with manganese were under 1 ppm. MeOH and blend fuels trace metal concentration results with manganese were under 2 ppm. RD and LFO fuels trace metal concentration results with lead were under 1 ppm. MeOH and blend fuels trace metals concentration results with lead were under 4 ppm. MeOH and blend

fuels trace metals concentration results with phosphorus and sulfur were under 4 ppm. MeOH and blend fuels trace metals concentration results with chromium, molybdenum and nickel were under 1 ppm. All the trace metals concentration results were below used determination limit of the ICP-OES methods.

5.7 Scanning electron microscope

The SEM images were taken from different places of the CS sample plates. The CS samples have not been scanned entirely. Figure 13 shows two unused CS plates that operate as the control samples for SEM results. The figure a) was neat and the figure b) was scruffy control. The figure b) shows fractionally tarnished spots. The neat and scruffy CS samples provide a baseline for comparison. The scruffy CS sample was naturally deteriorated.

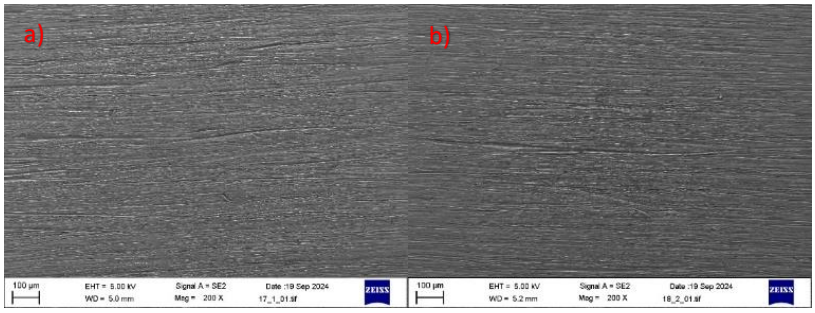

Figure 13. Two different unused CS samples as control. a) The neat and b) the scruffy CS sample controls.

The visual observation notices detectable tarnish on the sharper edge of each of the CS samples during both immersion tests. Figure 14 shows the tarnished edge of the CS sample on the immersion test at temperature of 23 °C, where fuel was MeOH.

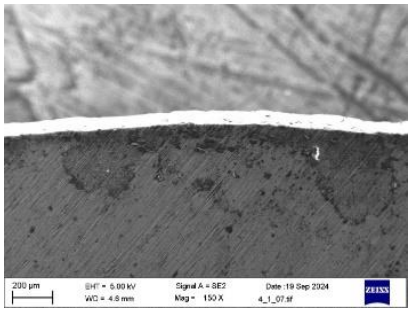

Figure 14. Tarnish edge of the CS sample of the immersion test at temperature of 23 °C and MeOH as fuel.

The rest of the SEM images are presented as sets of four images a), b), c) and d). The positions of the images in the CS samples remain the same in the series. Figure a) was a CS sample located at the bottom of the sample container. Figure b) was a hanging CS sample and the location of the SEM image was under the cotton thread. Figure c) was a hanging CS sample and the location of the SEM image was under the fuel surface and approximately 180° from the point in figure b). Figure d) is the control SEM images from Figure 9 a). The SEM images have enlargement of 200 times.

Figure 15 shows SEM images of the CS samples in RD fuel in the immersion test at temperature of 23 °C. All the locations a), b) and c) have fractionally tarnish points and d) is the CS control sample.

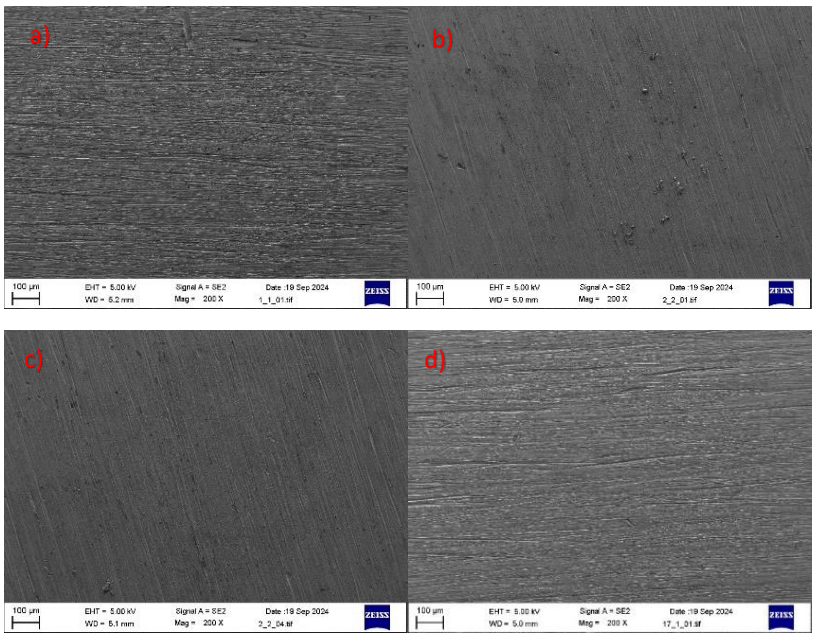

Figure 15. SEM images of the CS samples of the immersion test at temperature of 23 °C and RD as fuel. a) The CS sample from bottom of the sample container. b) The CS sample from hanging, location under the thread. c) The CS sample from hanging, location under the fuel, (180° from the b) location). d) The CS control image.

Figure 16 shows SEM images of the CS samples in MeOH fuel in the immersion test at temperature of 23 °C. SEM image a) was clear. SEM images b) and c) have fractionally tarnish points. SEM image d) is the CS control sample.

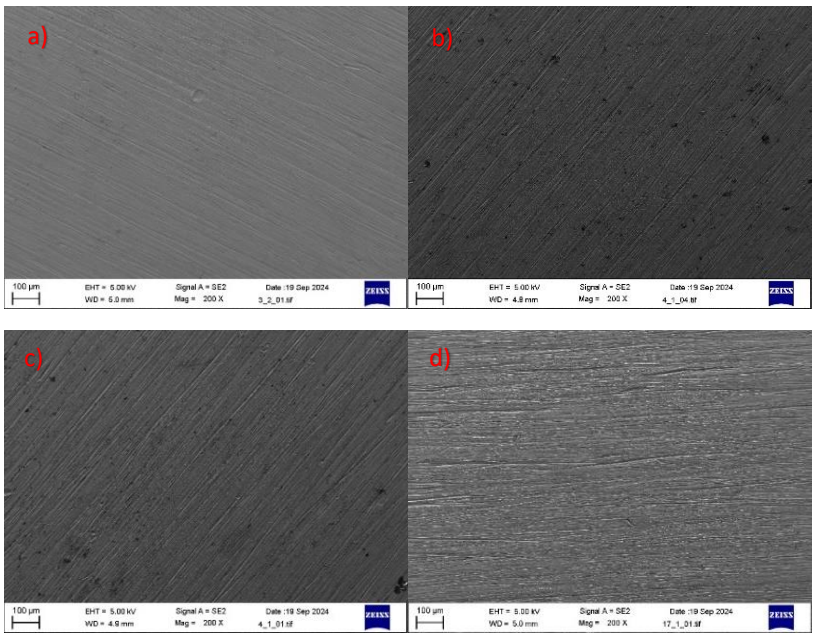

Figure 16. SEM images of the CS samples of the immersion test at temperature of 23 °C and MeOH as fuel. a) The CS sample from bottom of the sample container. b) The CS sample from hanging, location under the thread. c) The CS sample from hanging, location under the fuel, (180° from the b) location). d) The CS control image.

Figure 17 shows SEM images of the CS samples in fuel blend in the immersion test at temperature of 23 °C. SEM image a) was clear. SEM images b) and c) have fractionally tarnish points. SEM image d) is the CS control sample.

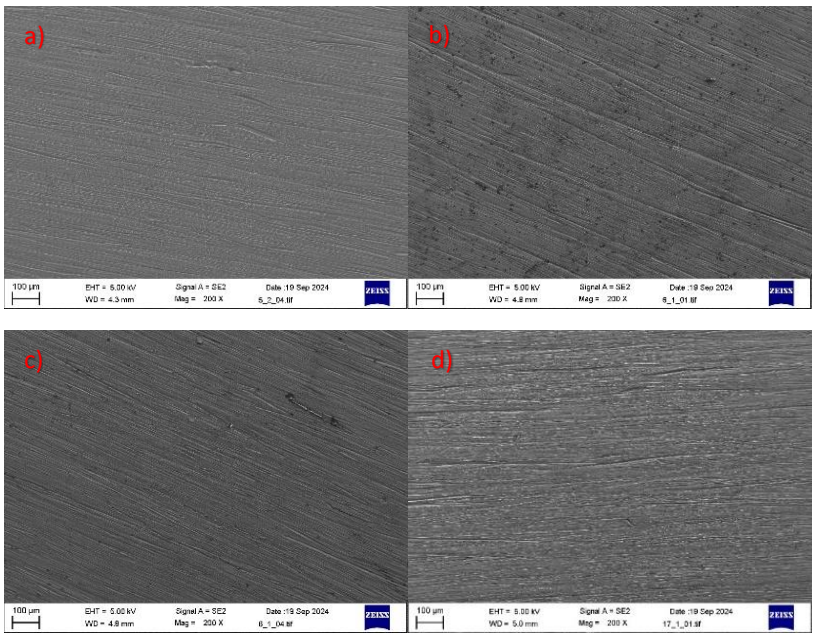

Figure 17. SEM images of the CS samples of the immersion test at temperature of 23 °C and fuel blends. a) The CS sample from bottom of the sample container. b) The CS sample from hanging, location under the thread. c) The CS sample from hanging, location under the fuel, (180° from the b) location). d) The CS control image.

Figure 18 shows SEM images of the CS samples in LFO fuel in the immersion test at temperature of 23 °C. SEM image a) was clear. SEM image b) considerably tarnish points. SEM image c) has fractionally tarnish points. SEM image d) is the CS control sample.

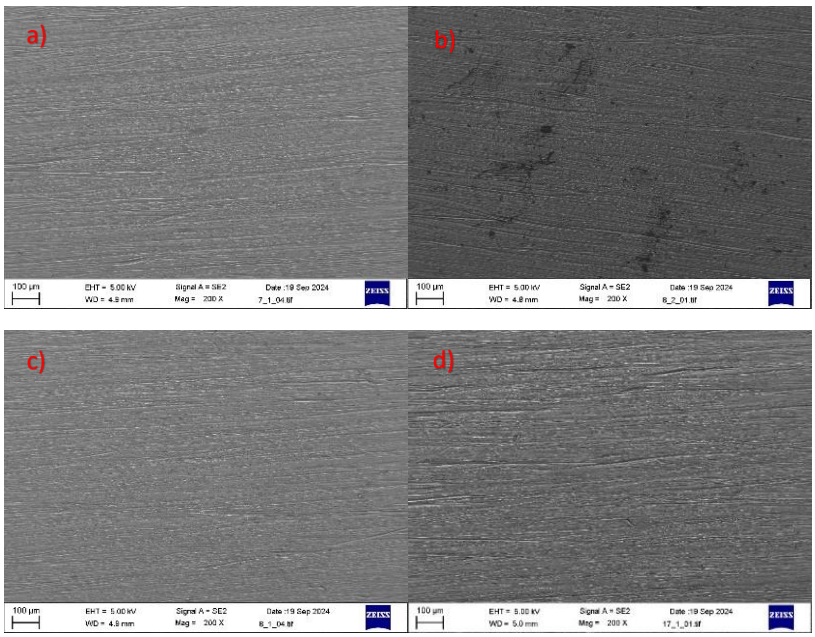

Figure 18. SEM images of the CS samples of the immersion test at temperature of 23 °C and LFO as fuel. a) The CS sample from bottom of the sample container. b) The CS sample from hanging, location under the thread. c) The CS sample from hanging, location under the fuel, (180° from the b) location). d) The CS control image.

Figure 19 shows SEM images of the CS samples in RD fuel in the immersion test at temperature of 40 °C. SEM images a) and b) were clear. SEM image c) has fractionally tarnish points. SEM image d) is the CS control sample.

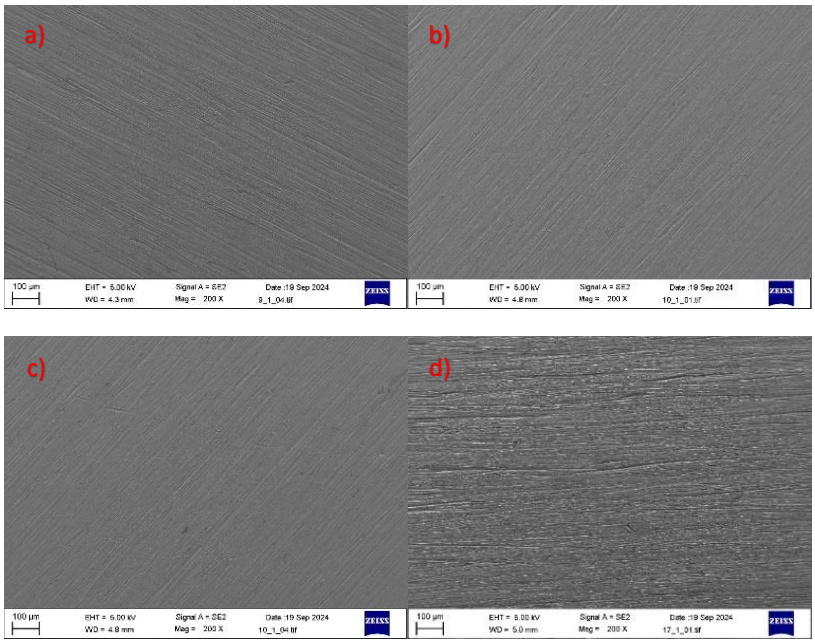

Figure 19. SEM images of the CS samples of the immersion test at temperature of 40 °C and RD as fuel. a) The CS sample from bottom of the sample container. b) The CS sample from hanging, location under the thread. c) The CS sample from hanging, location under the fuel, (180° from the b) location). d) The CS control image.

Figure 20 shows SEM images of the CS samples in MeOH fuel in the immersion test at temperature of 40 °C. SEM image a) was clear. SEM images b) and c) considerably tarnish points. SEM image d) is the CS control sample.

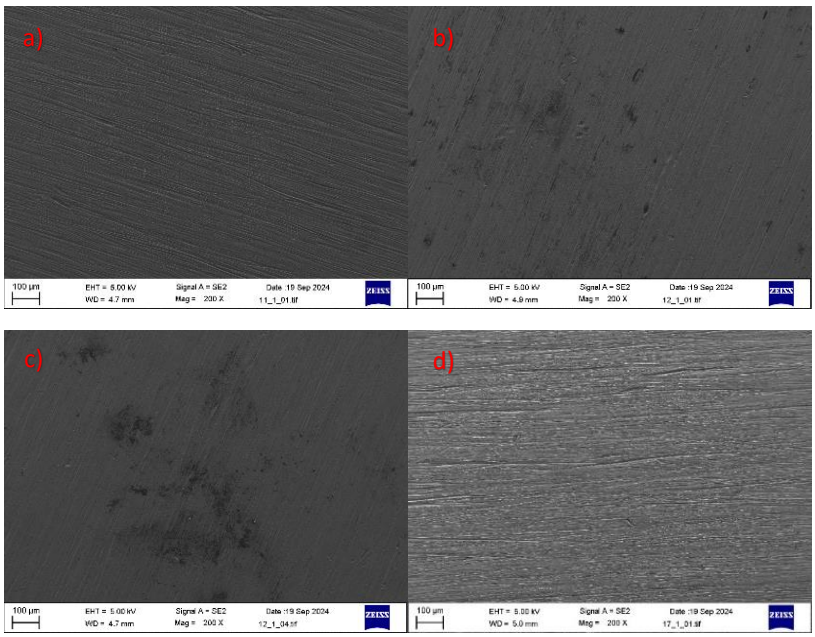

Figure 20. SEM images of the CS samples of the immersion test at temperature of 40 °C and MeOH as fuel. a) The CS sample from bottom of the sample container. b) The CS sample from hanging, location under the thread. c) The CS sample from hanging, location under the fuel, (180° from the b) location). d) The CS control image.

Figure 21 shows SEM images of the CS samples in fuel blend in the immersion test at temperature of 40 °C. SEM image a) was nearly clear. SEM images b) have fractionally tarnish points. SEM image c) have large areas of tarnish. SEM image d) is the CS control sample.

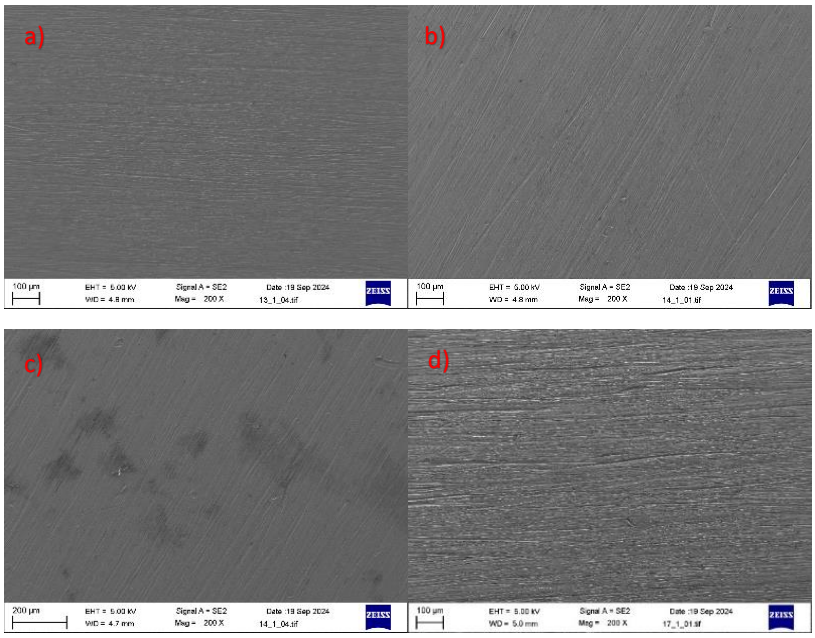

Figure 21. SEM images of the CS samples of the immersion test at temperature of 40 °C and blend as fuel. a) The CS sample from bottom of the sample container. b) The CS sample from hanging, location under the thread. c) The CS sample from hanging, location under the fuel, (180° from the b) location). d) The CS control image.

Figure 22 shows SEM images of the CS samples in LFO fuel in the immersion test at temperature of 40 °C. SEM image a) was clear. SEM images b) and c) have fractionally tarnish points. SEM image d) is the CS control sample.

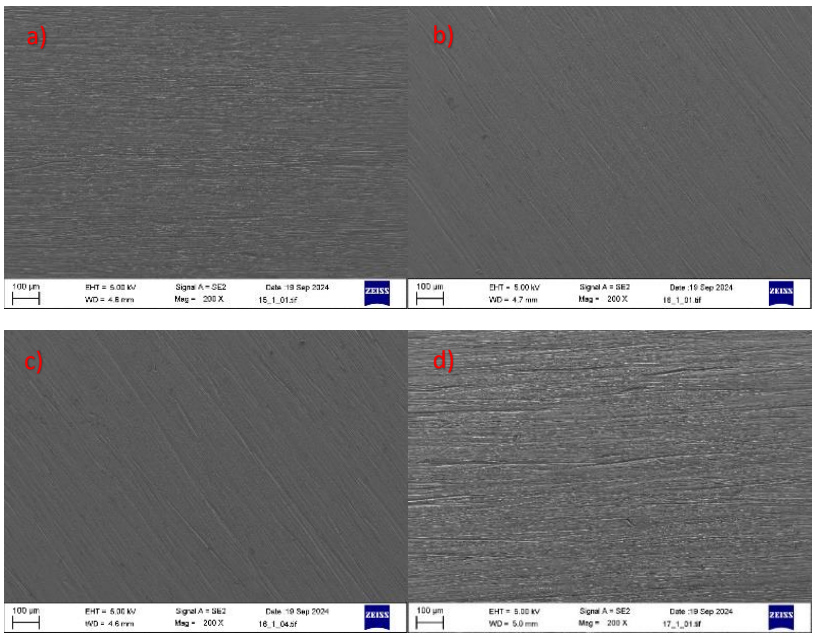

Figure 22. SEM images of the CS samples of the immersion test at temperature of 40 °C and LFO as fuel. a) The CS sample from bottom of the sample container. b) The CS sample from hanging, location under the thread. c) The CS sample from hanging, location under the fuel, (180° from the b) location). d) The CS control image.

6 Discussion

One of the most important targets of this master's thesis was to develop the immersion test procedure for the University of Vaasa's Fuel laboratory. The immersion test method was developed in sectors such as: the sample metal size, sample container and sample attachment method, fuel blend, temperature effect on the immersion tests results and SEM images.

A significant reduction of the size of the sample metal enables comparison of the sample weighing results before and after the immersion test. In previous immersion tests procedures in University of Vaasa's fuel laboratory, weighing results were inaccurate. It was possible to calculate the corrosion rate from the CS samples mass loss, as it was done in chapter 5.2 The carbon steel sample weights and corrosion rate. A reliable calculation of the corrosion rate requires a greater mass loss in the CS samples, than were obtained in the research results of this study. As a result of this study, the corrosion rate calculation model was created for the material compatibility method.

The shape of the metal sample and the hole in the middle, made it possible to hang the metal in the manner shown in Figure 23. In the design of the attachment the easy disassembly of the attachment after the end of the immersion test was considered. The CS sample was attached with a lint-free cotton thread in such a way that the sample cannot accidentally fall into the fuel during the removal phase. The cotton thread around the neck of the container and the opening of the container mouth were attached separately. The metal sample was attached with a special cotton thread in such a way that the metal sample rose from the fuel by lifting the ends of the thread. The attachment had a knot in the CS plate itself, so that the sample cannot fall if the other end of the cotton thread comes loose during the dismantling phase.

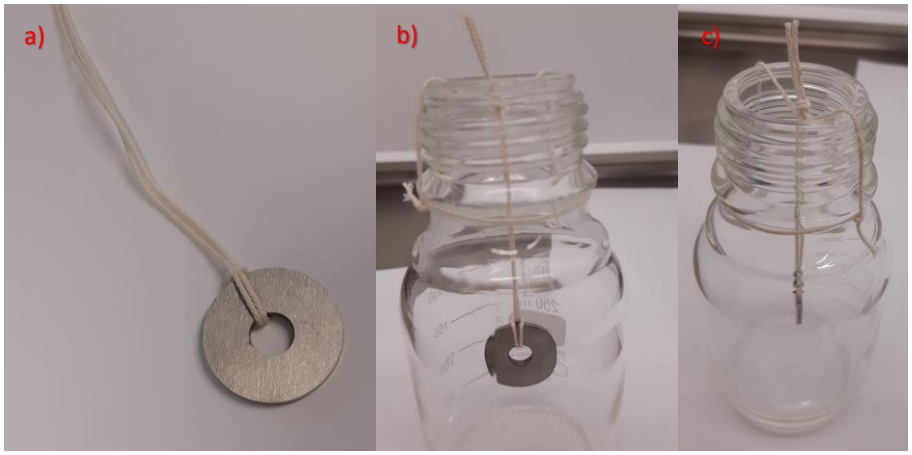

Figure 23. The method of fastening the metal sample for the sample container. a) The CS samples fastening method to cotton thread. b) and c) The method of attaching the CS sample to the sample container.

The fuel blend used in the implementation of the study has not previously been used as a fuel variant in an immersion test. The fuel blend had not been made in large quantities before, which led to changes in the blend ratio in both immersion tests, due to the ambient temperature.

In the Fuel laboratory of the University of Vaasa, a fume hood heating cabinet was acquired, which enabled two different temperatures of 23 °C and 40 °C. This made it possible to observe the effect of temperature on the occurrence of corrosion in immersion tests.

The SEM images enabled the visual examination of the CS samples from a close distance. The SEM image results created reliability and supported other analysis results.

According to the immersion tests results, the evaporation of MeOH and fuel blend cannot be concluded to have effect on the occurrence of corrosion. At temperature of 40 °C, the CS samples that were hang between the fuel and air interface, the mass losses were MeOH 0.00036 g and blend 0.00014 g. These were the biggest changes in terms of mass loss. When alcohol evaporates from the fuels, it could have affected the CS sample hanging in the air. However, the mass losses during the immersion tests were minor.

Based on the analysis results, the properties of MeOH and fuel blend kinematic viscosity and density remained almost the same despite the evaporation of the samples. As for the fuel blend, the kinematic viscosity increased slightly after both immersion tests. The evaporation of fuel blend has affected the mixture ratio, because MeOH and 1-octanol as alcohols have evaporated, while the amount of HVO remained approximately the same during the immersion tests. Evaporation of MeOH has no effect on the distillation curves in the immersion test at 23 °C. In the immersion test at 40 °C, MeOH IBP remained the same, but FBP increased slightly.

Based on a visual examination of the CS samples, it can be concluded that the untreated sharp edges and protrusions of the samples collected tarnish which cannot be confirmed as corrosion. The SEM images also did not confirm the tarnish as corrosion findings. The decrease in the weight of the CS samples during both immersion tests was minimal. The corrosion rate results calculated from weight loss excogitate the same conclusion.

Thangavelu et al. (2015, pp. 1–2) study calculated the corrosion rate from the immersion test with CS samples immersed in petro-diesel. The immersion test was executed at two different temperatures. The immersion test at room temperature 25-30 °C duration was 800 h. The calculated corrosion rate was 1.32797 µm/year (0.0523 mpy). The immersion test at temperature of 60 °C duration was 400 h. The calculated corrosion rate was 2.92 µm/year (0.115 mpy). Akhabue et al. (2014 pp. 546–547) research calculated the corrosion rate from the immersion test with mild CS samples immersed in diesel and petroleum diesel. The immersion test was executed in room temperature of 28 ± 2 °C and duration was 18 weeks meaning 3024 h. The calculated corrosion rate for diesel was 0.02793 µm/year (0.0011 mpy). The calculated corrosion rate for petroleum diesel was 2.28522 µm/year (0.09 mpy). However, comparing the *CR* results for Thangavelu et al. (2015) and Akhabue et al. (2014) studies, it can conclude that the obtained *CR* results from this study are low. In this study calculated *CR* for LFO was 0-0.17 µm/year. Other fuels *CR* results cannot compare with diesel fuel results. In this study MeOH has the highest *CR* result of 1.19 µm/year in the immersion test at temperature of 40 °C and

result is low according to highest levels of *CR* in Thangavelu et al. (2015) and Akhabue et al. (2014) studies. Formula 14 can be used to convert unit mpy to µm/year.

According to the measurement results of kinematic viscosity (Table 6) and density (Table 7), RD and blend fuels meet the requirements of the standard SFS-EN 15940. According to the measurement results of kinematic viscosity and density LFO fuels meet the requirements of the standard SFS-EN 590. MeOH does not meet the requirements of the SFS-EN 590 standard in terms of kinematic viscosity and density. However, the standard does not cover alcohol fuels.

Regarding the kinematic viscosity (Table 6), the results remain almost the same before and after both immersion tests for the fuels RD, MeOH and LFO. The main difference was between the fuel blends results. The amount of 1-octanol in the fuel blends was different in both immersion tests, which may explain the result. During the immersion tests the fuel blends also evaporated. In the first immersion test at temperature of 23 °C the properties of fuel blends with and without the CS samples were in line with each other. In the second immersion test at temperature of 40 °C the properties of fuel blends differ. The kinematic viscosity of fuel blend without the CS samples decreases and with the CS samples increases after the immersion test. The changes were small, but noticeable. The changes in the fuels kinematic viscosity results during the immersion tests was not significant enough to cause corrosion in the CS samples.

The density results remain almost the same before and after both immersion tests for all fuels RD, MeOH, blend and LFO (Table 7). The fuels density results during the immersion tests were not significant enough to cause corrosion in the CS samples.

RD fuel meets the SFS-EN 15940 standard limitations for fuels distillation properties (Table 9). The distillation curve of MeOH fuel does not meet the limits according to the standard SFS-EN 590. No distillation results were obtained for fuel blend, due to the PAC ISL OptiPMD analyzer limitation. LFO fuel meets the SFS-EN 590 standard limitations for

fuels distillation properties (Table 10). The results of the distillation tests of RD, MeOH and LFO fuels with non and the CS samples showed that IBP and FBP before and after both immersion tests remained nearly the same.

According to the Worldwide Fuel Charter (2019, pp. 5, 54) (WWFC) guidelines for trace metal concentrations such as copper, iron, manganese, sodium, phosphorus, lead, silicon and zinc concentration on diesel fuels are not limited. The use of additives with metal-based is prohibited. The WWFC guideline for trace metals concentration for gasoline should not transcend 1 ppm. WWFC guidelines are valid globally, disregarding the local fuel qualifications. Despite the fact that WWFC limitations are for gasoline, it can be considered indicative for diesels. After the immersion test, RD and LFO fuels meet the guidelines of WWFC demand for trace metal concentration in gasoline. MeOH and fuel blend do not meet the guidelines of WWFC demand for trace metal concentrations in gasoline after the immersion test.

Trace metal concentrations in Al, Cu, Fe, Mn, Si, V, Zn, Mn and Pb with both immersion tests results of RD, MeOH, blend and LFO fuels were comparable between each other's. Trace metal concentrations in Al, Cu, Fe, Mn, Si, V, Zn, Mn and Pb extent in the fuels were diminutive. Trace metal concentrations in P, S, Cr, Mo and Ni with both immersion tests results of MeOH and fuel blend were comparable between each other's. Trace metal concentrations in P, S, Cr, Mo and Ni extent in the fuels were diminutive.

Wang-Alho et al. (2024, pp. 1, 7) studied compatibility of HVO and MeOH blends with selected metals. The immersion test duration was 60 days in room temperature. The HVO trace metal concentration results before the immersion test for Al, Cu, Fe, Mn, Si, V, Zn and Pb were under 1 ppm (<1). The HVO trace metal concentration results after the immersion test for Al, Cu, Fe, Mn, V, Zn and Pb were under 1 ppm and Si was under 2 ppm. The MeOH trace metal concentration results after the immersion test with CS sample, the results for Al, Cu, Fe, Mn, V and Pb were under 1 ppm and for Si under 2 ppm. However, compering the HVO and RD trace metal concentration results before and

after the immersion tests from Wang-Alho et al. (2024) to this study, the results were similar. The only difference in trace metal concentration results was after the immersion test for Si. In the Wang-Alho et al. (2024) study the result was under 2 ppm and in this study under 1 ppm. Compering the MeOH and blend fuels trace metal concentration results before and after the immersion tests from this study to Wang-Alho et al. (2024) trace metal concentration result for MeOH, the results are similar. The difference in trace metal concentration results was Si and Pb. In this study the trace metal concentration result of Si was under 1 ppm and in the Wang-Alho et al. (2024) study the result was under 2 ppm. For the Pb the result was under 4 ppm and in the Wang-Alho et al. (2024) study the result was under 1 ppm. Kaivosoja (2023, pp. 2, 53) studied the effect of fuel contamination for selected metals. The LFO trace metal concentration results before the immersion test for Al, Cu, Fe, Mn, Si, V, Zn and Pb were under 1 ppm (<1). However, comparing the trace metal concentration results from Kaivosoja (2023) to this study, results were identical.

SEM images support the results of visual examination of the CS samples. Some of the CS samples figures showed fractionally or considerably areas of tarnish. According to SEM images, MeOH caused the most tarnish areas in the CS samples, especially in the immersion test at 40 °C. The visible tarnish in the SEM images cannot be concluded as corrosion. Based on the SEM images, the higher temperature of the immersion test at 40 °C may affect the greater number of tarnish areas. However, in the interpretation of SEM images, it should be noted that the CS sample plates were not completely reviewed. SEM images have pre-selected locations. SEM results do not therefore tell the overall situation of the sample.

Hou et al. (2023, pp. 7–8) corrosion study on cylinder liner on marine diesel engine SEM images shows easily noticeable traces caused by corrosion. In SEM images, corrosion can be seen as pits, cracks and deposition products (Figure 24). However, comparing SEM images from Hou et al. (2023) study to in this study SEM images (Figures 14-22), the tarnish areas cannot be determined as corrosion.

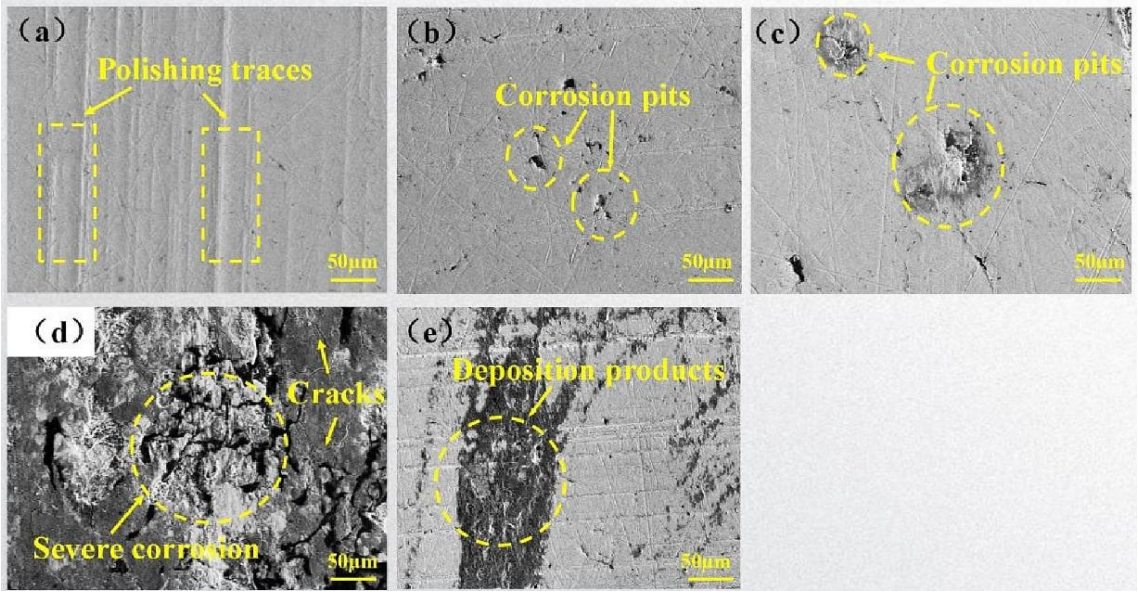

Figure 24. SEM images of corrosion in gray cast iron samples. a) Clean control with polishing traces. b) and c) Corrosion pits. d) Sever corrosion cracks. (e) Deposition products. (Hou et al., 2023, p. 8).

Study shows that at temperature of 23 °C or 40 °C of the immersion tests has minor or non-effect on the results. On the visual observation, in the immersion test at temperature of 23 °C in fuel blend the CS sample, which was fastened to hang the middle of fuel and air interface, had acquired tarnish changes in the inner arc of the sample hole 180° from the cotton thread (Figure 8). This change was not present at other temperatures or fuels. The change was not necessarily due to temperature. The mass loss of the CS samples was greater in the immersion test at temperature of 40 °C. The largest mass loss in MeOH fuel at 40 °C was 0.00036 g and the corrosion rate was 1.19 µm/year. Temperature of the immersion test did not affect the kinematic viscosity, density, distillation and measurements of the trace metal concentrations. SEM images have tarnished areas in both the immersion test temperatures. Based on the SEM images, a reliable interpretation cannot be made about the effect of temperature on the occurrence of corrosion in the CS samples.

Wang-Alho et al. (2024, p. 1) studied corrosion behavior. The immersion test with CS sample metal was conducted with HVO, MeOH and fuel blends with MeOH, HVO and 1-

octanol as adhesive. Wang-Alho et al. (2024) study shows similar results as this study, which elevates quality and reliability of this study.

This study has been carried out according to the ethical principles of scientific research, observing special caution and quality. The possibility of human and measurement error exists. Efforts have been made to reduce the possibility of error with various quality assurance methods, which were described in more detail in Chapter 4.3 Quality assurance of the methods. The results have been analyzed twice for quality assurance and to ensure the validity of the result. Analyzer's user manual and the manufacturer's instructions were used for sought to comply. Human errors may have occurred in weighing the CS samples, sample preparation, sample handling, solution preparation and pipetting. Potential samples contamination was possible during sample processing and analysis.

7 Conclusions

The first objective of this thesis was to improve the University of Vaasa's Fuel laboratory's immersion test initial setting. The second objective of the study was to implement the improved immersion test and examine the corrosion caused by RD, MeOH, blend and LFO fuels in CS and to examine the effect of temperature on the formation of corrosion.

Conclusions of the improvement of the immersion test:

- The improvement of the immersion test method enables a more detailed examination of the results of corrosion research.
- The smaller size of the CS samples allows the calculation of mass loss.
- The smaller size of the CS samples allows the calculation of corrosion rate.
- The shape of the CS samples enables the immersion test samples to be fastened in between the air and the fuels interface.
- The fastening practice in the immersion tests led to the evaporation of MeOH and fuel blend. The cotton thread stopped the lid of the sample container from sealing completely.
- Due to the ambient temperature fuels blend the mixing ratio differentiate.
- The heating cabinet made it possible to compare temperature differences of the immersion tests and to evaluate the effect of temperature on the occurrence of corrosion.
- SEM images allow inspection of the CS samples at close quarters of tarnish areas.

Conclusions of the immersion tests:

- Based on the study initial setting and the results, the fuels RD, MeOH, blend and LFO do not cause corrosion.
- The corrosion rate results were low.
- The RD and fuel blend meet the requirements of the SFS-EN 15940 standard based on the kinematic viscosity and density.

- The LFO fuel meets the requirements of the SFS-EN 590 standard based on the kinematic viscosity and density.
- The RD fuel meets the SFS-EN 15940 standard limitations for fuels distillation properties.
- The LFO fuel meets the SFS-EN 590 standard limitations for fuels distillation properties.
- Based on the results of the ICP-OES measurements, the CS samples did not contaminate the studied fuels.
- The results of the trace metal concentration measurements were in line with studies Wang-Alho et al. (2024) and Kaivosoja (2023).
- Based on both immersion tests analysis results of kinematic viscosity, density, distillation and ICP-OES measurements of the trace metal concentrations, the CS samples did not contaminate the studied fuels.
- Based on the visual observation of the CS samples, it can be concluded that the untreated sharp edges and protrusions of the samples collected tarnish areas, which cannot be confirmed as corrosion. The SEM images did not confirm the tarnished areas as corrosion findings.
- According to the SEM images the fuels did not cause corrosion in the CS samples during both immersion tests.
- According to the SEM images all fuels, notably MeOH, induced tarnish areas on the CS samples.
- Based on both immersion tests initial settings at temperature of 23 °C and 40 °C it was not possible to determine corrosion caused by temperature alteration on the CS samples and contamination of the fuels.
- Corrosion research of MeOH and fuel blend should be studied more.

The further research proposal is to continue the development of the immersion test procedure. In the implementation of the immersion test different fuels could be studied, including the immersion test of alternative fuels or fuels which are already in use. RD and MeOH blends with different adhesives and different blend rations could be studied.

ICE’s have many different metal grades and immersion tests with different metals are interesting subjects for further research. The immersion test could be modified with different temperatures and duration of the study.

The immersion test arrangement could be developed in several different ways. The lint-free cotton thread used in the immersion test and the attachment with the CS samples in the sample container caused problems with the seal between the lid and the container. This was shown in the evaporation of MeOH and blend fuels during the immersion tests. Further research proposal is to develop a fastening method, that does not allow the thread to get caught between lid and container spirals and allows the lid to be sealed properly. Standardization of the fuel blend production process in such a practice that blend ratio is the same in every immersion test. The sharper edges on the surfaces of the CS samples could be titivated and finished. The SEM image device can be equipped with an Energy Dispersive Spectroscope (EDS) elemental analysis for chemical and structural analysis. The CS samples tarnish areas shown in SEM images could be examined with EDS to reveal the content of tarnish with elemental analysis. In further studies, this feature could also be used to advantage.

In the practical implementation the normal operation of the ICE could be used as an analysis method and study the corrosion behavior of the ICE in the most natural environment possible. In this case the analysis method would consider temperature changes, moving parts, friction, variation in the quality of fuels, the cycle of refueling and combustion of fuel in an ICE, the effect of corrosion of small particles in the engine compartment, and the behavior of fuel in cold conditions.

8 Summary

Shipping is one of the fastest sources of greenhouse gas emissions and it uses a considerable amount of fossil fuels. Alternative fuels are future solutions for replacing fossil fuels. Examples among the possible alternative fuels that will be used in maritime applications in the future are hydrogen, ammonia, MeOH, HVO and their blends.

The compatibility of the alternative maritime fuels and materials has created challenges for shipping. ICE materials have different corrosion resistance. The durability and compatibility of the materials can be studied with various research methods. Corrosion caused by alternative fuels has been studied considerably. Corrosion causes challenges for ICE use. When the ICE is used, the fuel passes through the whole system. The fuel moves from the tank through the entire fuel system. Anywhere where fuel proceeds the material compatibility of alternative fuels must be ensured.

The first objective of this thesis was to improve the University of Vaasa's Fuel laboratory's immersion test initial setting. The second objective of the study was to implement the improved immersion test and examine the corrosion caused by RD, MeOH, blend and LFO in CS and to examine the effect of temperature on the formation of corrosion.

The improvement of the immersion tests was developed in sectors: the sample metal size, hang ability, sample container and sample attachment method, including the fuel blend for the immersion tests, temperature impact on the corrosion formation and SEM images. The improvement of the immersion test method enables a more detailed examination of the results of corrosion research.

The practical part of this study was to implement the improved method of the immersion tests to practice. The immersion test was conducted at two different temperatures of 23 °C and 40 °C. The CS samples were cleaned and weighed before the immersion tests. Four fuels were involved in the study: RD, MeOH, blend and LFO. In this study, there were two fuel samples containing the same fuel, one of which served as a control and the

second served as immersion test of the two CS samples. One of the CS samples was immersed in the bottom of the fuel sample container, the other was fastened with a lint-free cotton thread between the air and fuel interface. The duration of the first immersion test at temperature of 23 °C was 307 h. The duration of the second immersion test at temperature of 40 °C was 311 h.

After the immersion tests the CS samples were cleaned and weighed again. Visual observations of the corrosion were made. With results of weighing the mass loss was calculated of the CS samples. With mass loss of the samples, corrosion rate was calculated. Laboratory analysis methods of the fuels were kinematic viscosity, density, distillation and measurements of the trace metal concentrations. SEM images were taken from the CS samples to see the surface of the samples in more detail.

The calculated corrosion rate results were low. The kinematic viscosity and density results in both immersion tests RD and fuel blend meet the requirements of the SFS-EN 15940 and LFO the SFS-EN 590 standards. The distillation results in both immersion tests meet the requirements of the SFS-EN 15940 with RD fuels and the SFS-EN 590 with LFO fuels standard limitations. Based on all analysis results kinematic viscosity, density, distillation and measurements of the trace metal concentrations, it can be concluded that the CS samples did not cause material contamination for the RD, MeOH, blend and LFO fuels. According to the SEM images, the fuels did not cause corrosion in the CS samples during both immersion tests. According to the SEM images all fuels, notably MeOH, caused tarnish areas on the CS samples.

The results between immersion tests at 23 °C and 40 °C did not vary. Immersion tests at 23 °C or 40 °C did not make it possible to determine corrosion and fuel contamination due to temperature changes in the CS samples. Based on the results, the fuels RD, MeOH, blend and LFO do not cause corrosion on the CS samples.

References

Acar, C. & Dincer, I. (2020). The potential role of hydrogen as a sustainable transportation fuel to combat global warming. *International Journal of Hydrogen energy 45(2),* 3396–3406. https://doi.org/10.1016/j.ijhydene.2018.10.149

Ahn, S., Choi, Y., Kim, J. & Han, J. (2002). A study on corrosion resistance characteristics of PDV Cr-N coated steels by electrochemical method. *Surface and Coatings Technology 150(2–3),* 319–326. https://doi.org/10.1016/S0257-8972(01)01529-8

Akhabue, C., Aisien, F. & Ojo, C. (2014). The effect of Jatropha oil biodiesel on the corrosion rates of aluminium and mild carbon steel. *Biofuels 5(5),* 545–550. https://doi.org/10.1080/17597269.2014.1002995

Ampko Oy. (2017). *Abnaluneprüfzeugnis des Liferanten nach DIN EN 10204-3.1.* Retrieved July 31, 2024, from Ampko Oy.

Anton Paar. (n.d.). *SVM 3000 Stabinger Viscometer.* Anton Paar. Retrieved August 1, 2024, from https://photos.labwrench.com/equipmentManuals/1798-446.pdf

ASTM International. (2017). Standard Practice for Preparing, Cleaning, and Evaluating Corrosion Test Specimens. (ASTM G1 – 03).

Ateeq, M., Li, L., Abdullah, M., Ahmed, A., Gohar, G., Rafiq, M., Rauf, S., Ali, A. & Saleem, H. (2022). Evaluating corrosion effect of biodiesel produced from neem oil on automotive materials. *Materials Today Sustainability 18,* 1–8. https://doi.org/10.1016/j.mtsust.2022.100130

Avtotachki. (2022). *Koeajon auton polttoaine: biodiesel OSA 2.* Retrieved August 1, 2024, from https://fi.avtotachki.com/avtomobil-noe-toplivo-biodizel-chast-2/

Bejinariu, C., Burduhos-Negis, D-P. & Cimpoesu, N. (2020). Immersion Behavior of Carbon Steel, Phosphate Carbon Steel and Painted Carbon Steel in Saltwater. *Materials 14(1),* 1–21. https://doi.org/10.3390/ma14010188

BG Suomi (n.d.). *Ruostetta moottorissa; Liian hapokasta luettavaksi.* JoyDrive Oy. Retrieved August 1, 2024, from https://bgprod.fi/ruostetta-moottorissa-liian-hapokasta-luettavaksi/

Bruun, N. (2022*). Bio-oils in Contact with Steels and Copper Surfaces.* [Doctoral dissertation, Åbo Academi University]. Doria.

https://www.doria.fi/bitstream/handle/10024/186209/bruun_nina.pdf?sequence=1&isAllowed=y URN:ISBN_978-952-12-4203-8

Cames, M., Wissner, N. & Sutter, J. (2021, June). *Ammonia as a marine fuel. Risks and perspectives.* Öko-Institut e.V. Retrieved August 8, 2024, from https://en.nabu.de/imperia/md/content/nabude/verkehr/210622-nabu-study-ammonia-marine-fuel.pdf

Det Norske Veritas. (2024). *Maritime forecast to 2050*. DNV. Retrieved September 11, 2024, from https://www.dnv.com/maritime/publications/maritime-forecast/

Durbin, D.J. & Malardier-Jugroot, C. (2013). Review of hydrogen storage techniques for on board vehicle applications. *International Journal of Hydrogen Energy 38(34),* 14595–14617. https://doi.org/10.1016/j.ijhydene.2013.07.058

Ellis J. & Tanneberger K. (2015). Study on the use of ethyl and methyl alcohol as alternative fuels in shipping. Göteborg: SSPA. Retrieved July 22, 2024, from http://www.emsa.europa.eu/newsroom/latest-news/item/2726-study-on-the-use-of-ethyl-and-methyl-alcohol-as-alternative-fuels-in-shipping.html

European Technology and Innovation Platform ETIP Bioenergy. (2020). *Bioenergy Fact Sheet: Hydrogenated vegetable oil (HVO).* ETIP Bioenergy. Retrieved September 10, 2024, from https://etipbioenergy.eu/images/ETIP_B_Fact-sheet_HVO_feb2020.pdf

European parliament. (2022, June 15). *Emissions from planes and ships: facts and figures (infographic).* Topics European Parliament. Retrieved July 8, 2024, from https://www.europarl.europa.eu/topics/en/article/20191129STO67756/emissions-from-planes-and-ships-facts-and-figures-infographic

Foretich, A., Zaimes, G., Hawkins, T. & Newes, E. (2021). Challenges and opportunities for alternative fuels in the maritime sector. *Maritime Transport Research 2,* 1–27. https://doi.org/10.1016/j.martra.2021.100033

Heikkinen, E-P. & Tanskanen, P. (2022, January 1). *Scanning Electron Microscopy (SEM). Characterisation methods of inorganic materials.* Retrieved October 15, 2024, from http://cc.oulu.fi/~kamahei/m/477426S/CMIM-SEM.pdf

Helander, B. (2021, April 26). *Merten mirai – maailman ensimmäinen vetykäyttöinen matkustaja-autolautta tähtää liikenteeseen 2027.* Moottori. Retrieved August 24, 2024, from https://moottori.fi/uutinen/merten-mirai-maailman-ensimmainen-vetykayttoinen-matkustaja-autolautta-tahtaa-liikenteeseen-2027/

Herbinet, O., Bartocci, P. & Dana, A. (2022). On the use of ammonia as a fuel – A perspective. Fuel Communications 11, 1–16. https://doi.org/10.1016/j.jfueco.2022.100064

Hilbers, T., Sprakel, L., van den Enk, L., Zaalberg, B., van den Berg, H. & van den Ham, L. (2015). Green Diesel from Hydrotreated Vegetable Oil Process Design Study. *Chemical Engineering & Technology 38(4),* 651–657. http://doi.org/10.1002/ceat.201400648

Hoang, A., Tabatabaei, M. & Aghbashlo, M. (2020). A review of the effect of biodiesel on the corrosion behavior of metals/alloys in diesel engines. *Energy Sources, Part A: Recovery, Utilization, and Environmental Effects 42(23),* 2923–2943. http://doi.org/10.1080/15567036.2019.1623346

Hou, X., Wang, Y., Dai, L., Yang, Y., Du, J., Wang, Y. & Wan, H. (2023). Study on the corrosion and wear behaviors of cylinder liner in marine diesel engine burning low sulfur fuel oil. *Engineering Failure Analysis 147,* 1–17. https://doi.org/10.1016/j.engfailanal.2023.107151

Hänninen, H., Karppinen, M., Leskelä, M. & Pohjakallio, M. (2022). *Tekniikan kemia.* [Finland Otavan kirjapaino Oy] (16. ed.). Edita. ISBN:978-951-37-8664-9.

IRENA & Methanol Institute. (2021). Innovation Outlook: Renewable Methanol. Retrieved July 22, 2024, from https://www.irena.org/-/media/Files/IRENA/Agency/Publication/2021/Jan/IRENA_Innovation_Renewable_Methanol_2021.pdf

Jaarinen, S. & Niiranen, J. (2005). *Laboratorion analyysitekniikka.* [Edita Oppiminen Oy] (5. ed.). Edita. ISBN:978-951-37-4445-8.

Kaivosoja, J. (2023). *Polttoainekontaminaation vaikutukset valikoiduille metalliseoksille.* [Master's thesis, University of Vaasa]. Osuva.

https://osuva.uwasa.fi/bitstream/handle/10024/16397/Uwasa_2023_Kaivosoja_Jonna.pdf?sequence=2&isAllowed=y

Kim, M.-S. & Chun, K. (2023). A Comprehensive Review on Material Compatibility and Safety Standards for Liquid Hydrogen Cargo and Fuel Containment System in Marine Applications. *Journal of marine science and engineering 11(10),* 1–35. https://doi.org/10.3390/jmse11101927

Kuittinen, T. (2012). *Biopolttoaineiden ominaisuudet.* [Bachelor's thesis, University of Lappeenranta]. LUTPub. https://lutpub.lut.fi/bitstream/handle/10024/88854/Biopolttoaineiden%20ominaisuudet.pdf?sequence=1

Kyriakou, V., Garagounis E., Vasileiou A. & Stoukides M. (2017). Progress in the Electrochemical Synthesis of Ammonia. *Catalysis Today 286,* 2–13. http://doi.org/10.1016/j.cattod.2016.06.014

Liu, Z., Guo, Z., Rao, X., Xu, Y., Sheng, C. & Yuan, C. (2022). A comprehensive review on the material performance affected by gaseous alternative fuels on internal combustion engines. *Engineering Failure Analysis 139,* 1–19. https://doi.org/10.1016/j.engfailanal.2022.106507

Mankonen, A. (2014). *Bioöljy ja pyrolyysi.* [Bachelor thesis, University of Lappeenranta]. LUTPub. https://lutpub.lut.fi/bitstream/handle/10024/96513/Kandidaatinty%C3%B6_Aleksi_M_bio%C3%B6ljy_ja_pyrolyysi.pdf

Marine & Offshore. (2024). *Ammonia.* Home – Expertise for Sustainability – Marine Future Fuels. Retrieved August 9, 2024, from https://marine-offshore.bureauveritas.com/shipping-decarbonization/future-fuels/ammonia

Mettler Toledo. (2013). *Operating Instructions. Excellence Analytical Balances.* Retrieved September 2, 2024, from https://www.mt.com/dam/P5/labtec/02_Analytical_Balances/04_XS/03_Documentations/03_Operating_Instructions/OI_XS_Analytical_Part_1_EN.pdf

MMM Group. (2012). *Instructions for use.* Retrieved September 3, 2024, from https://www.revodix.co.kr/wp-content/uploads/2015/07/LSI_S_np_en-1309_mmm_V2.10_B2V.pdf

Mussa, N-S., Toshtay, K. & Capron, M. (2024). Catalytic Applications in the Production of Hydrotreated Vegetable Oil (HVO) as a Renewable Fuel: A Review. *Catalysts 14(7),* 1–27. https://doi.org/10.3390/catal14070452

Mäkelä, M., Soininen, L., Tuomola, S. & Öistämö, J. (2020). Tekniikan kaavasto. [Bookwell Oy] (21. ed.). Tammertekniikka. ISBN 978-952-5491-48-7

Niemi, S. & Ovaska, T. (n.d.) Mäntämoottorien rakenteesta. Moodle [Restricted access]. Retrieved October 6, 2024, from https://learn.uwasa.fi/my/

Neste. (2023). *SAFETY DATA SHEET. Neste Renewable Diesel; Neste Renewable Diesel 100 %; Neste MY Renewable Diesel.* Retrieved September 15, 2024, from https://www.neste.com/files/pdf-en-us/4VNjQZidFKU4f2q7jaKONx-13898_usa.pdf

Neste. (n.d.) *NEXBTL-teknologia.* NEXBTL tuotteet. Retrieved September 19, 2024, from https://www.neste.fi/konserni/tietoa-meista/tuotanto/nexbtl-teknologia

Okokpujie, I., Ojo, A., Adaramola, B., Oladimeji, M., Ogundele, R. & Abiodun, C. (2023). Study of Corrosion, and Thermal Analysis of Materials for Internal Combustion Engines and their Compatibility: A Review. *IOP Conference Series: Earth and Environmental Science 1322,* 1–20. https://doi.org/10.1088/1755-1315/1322/1/012007

Oni, B., Sanni, S., Ezurike, B. & Okoro, E. (2022). Effect of corrosion rates of preheated Schinzochytrium sp. microalgae biodiesel on metallic components of a diesel engine. *Alexandria Engineering Journal 61(10),* 7509–7528. https://doi.org/10.1016/j.aej.2022.01.005

Oy Linde Gas Ab. (2024) *Vety. Käyttöturvallisuustiedote.* Käyttöturvallisuustiedotteet. Tiedostonimi: SDS_000010021694_FI_FI.PDF. Retrieved July 25, 2024, from https://www.linde-gas.fi/shop/LINSafetyDataSheetsView?catalogId=3074457345616682368&storeId=715851185&langId=-1005&&catalogId=3074457345616682368&

PAC. (2019). *OptiPMD Next-Generation Lab Micro Distillation Analyzer.* Retrieved August 1, 2024, from https://www.paclp.com/tenants/pac/documents/optipmd%20brochure%20us%20rev5.pdf

Peda.net. (2018). *Korroosio.* Retrieved August 14, 2024, from https://peda.net/sievi/sievin-lukio/oppiaineet2/kemia/kemia41/tkapp/luku-4-1b:file/download/29a93edefc9c68149118c12444a505a05e55cceb/Materiaalit_ja_teknologia_KE4_LUKU4.1b.pdf

Rufer, A. (2022). Quantitative Design of a New e-Methanol Production Process. *Energies 15(24),* 1–14. https://doi.org/10.3390/en15249309

Finnish Standards Association. (2014). Automotive fuels. Determination of manganese and iron content in diesel. Inductively coupled plasma optical emission spectrometry (ICP OES) method. (SFS-EN 16576).

Finnish Standards Association. (2017). *Automotive fuels. Diesel. Requirements and test methods.* (SFS-EN 590:2013 + A1:2017).

Finnish Standards Association. (2023). *Automotive fuels. Paraffinic diesel fuel from synthesis or hydrotreatment. Requirements and test methods.* (SFS-EN 15940:2023:en).

Shehzad, A., Ahmed, A., Quazi, M., Jamshaid, M., Rahman, A., Hassan, M., & Javed, H. (2021). Current Research and Development Status of Corrosion Behavior of Automotive Materials in Biofuels. *Energies, 14(5),* 1–36. https://doi.org/10.3390/en14051440

Shiva Kumar, S. & Himabindu, V. (2019). Hydrogen production by PEM water electrolysis – A review. *Material Science for Energy Technologies 2(3),* 442–454. https://doi.org/10.1016/j.mset.2019.03.002

Sirviö, K., Nuortila, C., Niemi, S., Ovaska, T., & Heikkilä, S. (2023, June 12–16). The corrosion behavior of steels in contact with metal doped biodiesel-diesel blends. CIMAC Congress Busan, 1–9 Retrieved October 3, 2024, from https://www.cimac.com

Thangavelu, S., Chelladorai, P. & Ani, F. (2015). Corrosion Behaviour of Carbon Steel in Biodiesel-Diesel-Ethanol (BDE) Fuel Blend. *MATEC Web of Conference 27,* 1–4. https://doi.org/10.1051/matecconf/20152701011

Tukes. (2024) *Vedyn käsittelyn ja varastoinnin turvallisuus.* Retrieved August 26, 2024, from https://tukes.fi/vedyn-kasittelyn-ja-varastoinnin-turvallisuus

VWR BDH Chemicals. (n.d.-a). *Käyttöturvallisuustiedote.* Retrieved August 8, 2024, from https://fi.vwr.com/assetsvc/asset/fi_FI/id/7668340/contents

VWR BDH Chemicals. (n.d.-b). *Käyttöturvallisuustiedote.* Retrieved August 8, 2024, from https://fi.vwr.com/assetsvc/asset/fi_FI/id/7896964/contents

Wang-Alho, H., Sirviö, K., Nuortila, C., Kaivosoja, J., Mikulski, M. & Niemi, S. (2024). Compatibility of Methanol-Hydrotreated Vegetable Oil Blends with Chosen Steels and Aluminum. *Energies 17(14),* 1–16. https://doi.org/10.3390/en17143423

Worldwide Fuel Charter. (2019). Worldwide Fuel Charter Gasoline and Diesel Fuel. Retrieved November 2, 2024, from https://www.acea.auto/files/WWFC_19_gasoline_diesel.pdf

Worldwide Fuel Charter. (2009). Biodiesel Guidelines. Retrieved December 22, 2024, from https://www.acea.auto/uploads/publications/20090423_B100_Guideline.pdf

Zafar, F., Ghousal, A., & Sharmin, E. (Ed.) (2022). Corrosion Fundamentals and Protection Mechanisms. IntechOpen. http://dx.doi.org/10.5772/intechopen.94634

Zemite, L., Jansons, L., Zeltins, N., Lappuke, S. & Bode, I. (2023). Blending Hydrogen with natural gas/biomethane and transportation in existing gas network. *Latvian journal of physics and technical sciences 60(5),* 43–55. https://doi.org/10.2478/lpts-2023-0030